NAVAL POSTGRADUATE SCHOOL
MONTEREY, CALIFORNIA

THESIS

A TACTICAL APPLICATION OF COASTAL ACOUSTIC TOMOGRAPHY

by

Jeroen Franken

December, 1994

Thesis Advisor: James H. Miller

Approved for public release; distribution is unlimited.

DISCLAIMER NOTICE

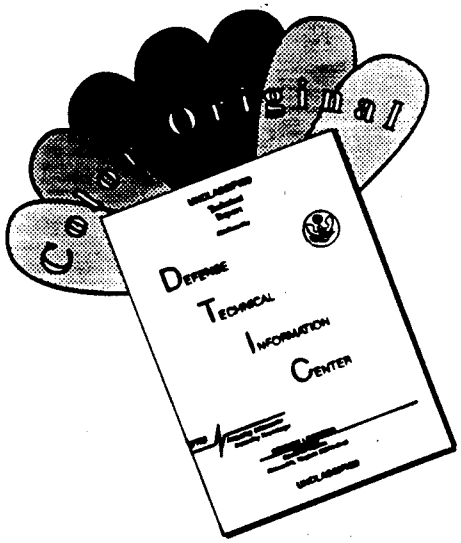

THIS DOCUMENT IS BEST QUALITY AVAILABLE. THE COPY FURNISHED TO DTIC CONTAINED A SIGNIFICANT NUMBER OF COLOR PAGES WHICH DO NOT REPRODUCE LEGIBLY ON BLACK AND WHITE MICROFICHE.

REPORT DOCUMENTATION PAGE

Form Approved OMB No. 0704-0188

1. AGENCY USE ONLY *(Leave blank)*	2. REPORT DATE December, 1994	3. REPORT TYPE AND DATES COVERED Master's Thesis

4. TITLE AND SUBTITLE A TACTICAL APPLICATION OF COASTAL ACOUSTIC TOMOGRAPHY (UNCLASSIFIED)

5. FUNDING NUMBERS

6. AUTHOR(S) JEROEN FRANKEN

7. PERFORMING ORGANIZATION NAME(S) AND ADDRESS(ES)
Naval Postgraduate School
Monterey CA 93943-5000

8. PERFORMING ORGANIZATION REPORT NUMBER

9. SPONSORING/MONITORING AGENCY NAME(S) AND ADDRESS(ES)

10. SPONSORING/MONITORING AGENCY REPORT NUMBER

11. SUPPLEMENTARY NOTES The views expressed in this thesis are those of the author and do not reflect the official policy or position of the Department of Defense, the U.S. Government or the Royal Netherlands Navy.

12a. DISTRIBUTION/AVAILABILITY STATEMENT
Approved for public release; distribution is unlimited.

12b. DISTRIBUTION CODE

13. ABSTRACT *(maximum 200 words)*

The objective of this study is to investigate the utility of acoustic tomography for performance assessment of a generic low frequency active sonar system. The performance of the sonar is simulated using tomography-derived sound speed data versus a range independent ocean model. The ocean environment used in the simulation is 159 tomographic snapshots of the Barents Sea Polar Front, taken every 5 minutes in August 1992. The modeled sonar system consists of a 1000 Hz source with a source level of 205.5 dB and a towed horizontal array of hydrophones. The system is derived from unclassified parameters of ATAS (Active Towed Array Sonar), built by Thomson Sintra ASM and British Aerospace SEMA, and the experimental ALF sonar, designed by FEL-TNO (the Netherlands) and built by Thomson Sintra ASM. The tomographic images over a range of 26 km provide a realistic ocean in which system performance is assessed. This study used a broadband, coupled normal mode, propagation model and assumed a noise-limited condition. The probability of detection calculated as a function of time for 13 hours is compared with that estimated using a range- and time-independent assumption. The utility of coastal acoustic tomography for tactical applications is discussed.

14. SUBJECT TERMS Low frequency active sonar performance, ATAS, experimental ALF sonar, Coastal Acoustic Tomography.

15. NUMBER OF PAGES 65

16. PRICE CODE

17. SECURITY CLASSIFICATION OF REPORT	18. SECURITY CLASSIFICATION OF THIS PAGE	19. SECURITY CLASSIFICATION OF ABSTRACT	20. LIMITATION OF ABSTRACT
Unclassified	Unclassified	Unclassified	UL

Approved for public release; distribution is unlimited.

A TACTICAL APPLICATION OF COASTAL ACOUSTIC TOMOGRAPHY

by

Jeroen Franken
Lieutenant Commander, Royal Netherlands Navy
Royal Netherlands Naval College, 1982

Submitted in partial fulfillment
of the requirements for the degree of

MASTER OF SCIENCE IN ENGINEERING ACOUSTICS

from the

NAVAL POSTGRADUATE SCHOOL
December 1994

Author: _____
Jeroen Franken

Approved by: _____
James H. Miller, Thesis Advisor

_____
Ching-Sang Chiu, Thesis Co-Advisor

_____
Warren W. Denner, Thesis Co-Advisor

_____
Anthony A. Atchley, Chairman
of the Engineering Acoustics Academic Committee

ABSTRACT

The objective of this study is to investigate the utility of acoustic tomography for performance assessment of a generic low frequency active sonar system. The performance of the sonar is simulated using tomography-derived sound speed data versus a range independent ocean model. The ocean environment used in the simulation is 159 tomographic snapshots of the Barents Sea Polar Front, taken every 5 minutes in August 1992. The modeled sonar system consists of a 1000 Hz source with a source level of 205.5 dB and a towed horizontal array of hydrophones. The system is derived from unclassified parameters of ATAS (Active Towed Array Sonar), built by Thomson Sintra ASM and British Aerospace SEMA, and the experimental ALF sonar, designed by FEL-TNO (the Netherlands) and built by Thomson Sintra ASM. The tomographic images over a range of 26 km provide a realistic ocean in which system performance is assessed. This study used a broadband, coupled normal mode, propagation model and assumed a noise-limited condition. The probability of detection calculated as a function of time for 13 hours is compared with that estimated using a range- and time-independent assumption. The utility of coastal acoustic tomography for tactical applications is discussed.

ACKNOWLEDGEMENT

The broadband coupled normal mode code used in this study was developed by C.-S. Chiu under the sponsorship of EOS Research Associates of Monterey, California. The author would like to thank Dr W.W. Denner for making this code available to him.

TABLE OF CONTENTS

I. INTRODUCTION

Since its introduction by Munk and Wunsch (1979), ocean acoustic tomography has evolved from the experimental phase into a phase in which different applications are feasible (Miller and Franken, 1994). Besides being of significant interest to oceanographic institutes, acoustic tomography can have applications for the world's navies. They need range dependent propagation prediction models to assess the sonar performance in ocean areas with complicated Sound Speed Profiles (SSP). The increased importance of anti-submarine warfare in coastal ocean regions of the world requires more accurate and timely sound speed maps. Acoustic tomography can be utilized to provide space and time dependent maps of the ocean sound speed field.

In order to quantify the above need for range and time dependent SSP's, sonar performance assessment using acoustic tomography derived SSP's is compared to the assessment using a conventional, range independent method, e.g. the use of expendable bathythermograph (XBT) data. The objective of this study is therefore **to compare the sonar performance assessment of a low frequency active sonar system using tomography-derived sound speed data versus a range independent ocean model in order to show the utility for acoustic tomography as a tool for long range sonar performance evaluation.**

The tomographic and XBT ocean models are compared. The ocean environment used in the simulation is 159 tomographic snapshots of the Barents Sea Polar Front (every 5 minutes) taken in August 1992. The fixed location of the experiment is the Barents Sea Polar Front about 50 nm east of Bear Island (Figure 1). In the study, a 1000 Hz active sonar system with an acoustic power of 1 kW is assumed. The sonar performance assessment is quantified by the probability of detection on a

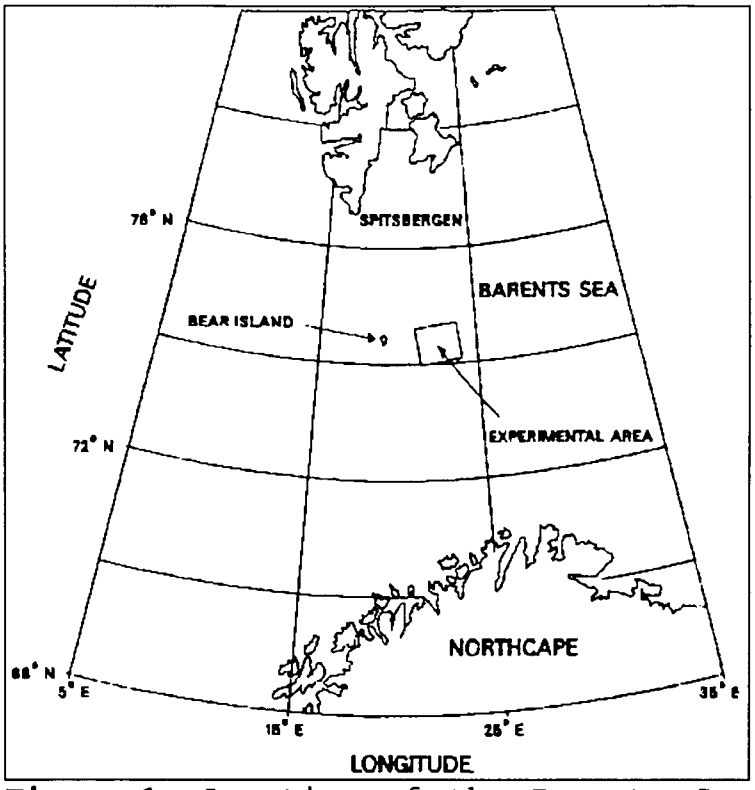

Figure 1. Location of the Barents Sea Polar Front Experiment by the NPS, WHOI and SAIC in August 1992 (Miller, J.H. et al., 1994).

submarine with a target strength of 10 dB.

First the environmental setting of this study is described in Chapter II, "The Imaged Ocean." In Chapter III the hypothetical sonar system used for the comparison of the models is described. All parameters of the sonar are derived from unclassified data and, though the numbers are fictitious, they represent realistic figures for a modern low frequency active sonar system. Chapter IV deals with the transmission loss calculations by a coupled mode approach. The transmission loss for both, the range dependent and range independent, models is calculated using the same code. Finally the resulting probability of detection for noise-limited conditions is presented in Chapter V, followed by some concluding remarks in Chapter VI.

II. THE IMAGED OCEAN

A. WHY A RANGE DEPENDENT MODEL?

In order to calculate the sonar performance assessment, we have to choose an appropriate acoustic model that is valid for the area of operation and requires a reasonable amount of computer calculation time. Since it is impossible in a real ocean to calculate exactly the real parameters, any model is an estimate. In general, range independent models are simpler, require less computing time, but are less accurate in range varying conditions.

When we deal with range and time varying oceanographic conditions, we prefer a model that includes the variability of the conditions as a function of range and for which the calculations can be performed within the characteristic time slot of the changing conditions. In this case we need a range dependent model, that requires regular inputs of the changing conditions and fast calculations.

Standard routine on board naval ships is to measure the acoustic conditions locally with an XBT or sound velocity meter (XSV). Usually, this is done in the operation area in six hour intervals or when the acoustic conditions may have changed substantially. We can use the resulting SSP as input for a range independent model. This method does not take into account the range variability of the ocean when we deploy long range sonar systems. For short range sonar though, this method can be adequate, since the range variability of the ocean is often negligible for these short ranges. We also can use the SSP's of several ships at different locations as the input for a range dependent model. But still this method does only use spot measurements and does not take the time variability of the ocean into account.

Sonar predictions for a long range sonar system in an ocean with varying acoustic conditions, e.g. near an

oceanographic front, require a range dependent model with inputs of sufficient range and time resolution. These inputs can be provided by ocean acoustic tomography.

B. OCEAN ACOUSTIC TOMOGRAPHY

Ocean acoustic tomography is an efficient method to measure current or sound speed fields over a large ocean volume, described by Miller and Franken (1994), Spindel and Worcester (1990), and many others. It is based on travel time perturbations between sources and receivers of acoustic signals traveling along different paths.

Acoustic tomography uses few transmitters and receivers to form a network of crossing raypaths in a horizontal area (Figure 2). By transmitting acoustic signals from one transmitter to any receiver over multiple paths in the vertical plane, one can deduce the properties of the ocean's interior in this plane on the basis of how the ocean altered the signals. Combining the information of all vertical slices

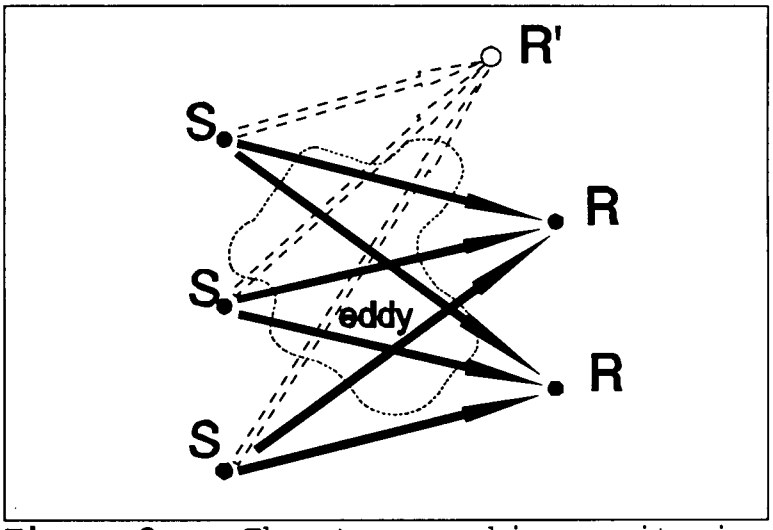

Figure 2. The tomographic monitoring system: transducers (S) and receivers (R). Addition of one receiver (R') increases the number of acoustic paths multiple times.

of the network enables us to derive a three dimensional image, much like the medical CT scan.

Adding more transducers or receivers increases the number of slices at a rate much greater than achieved with conventional instruments that do not collect data from crossing paths. By using transceivers, even more paths can be used and two way measurements can be done, enabling determination of current fields. Moreover these measurements are performed at the speed of sound, about 3000 knots in water, much faster than any research vessel can sail. It enables us to obtain a nearly continuous update of the ocean structure.

Acoustic tomography can provide continuous, nearly real time information to predict sonar performance and counter detection ranges in a fixed area. Sometimes naval forces are required to operate in one area for a prolonged period of time. In these circumstances task group commanders need continuous information of the changing environment in this unchanging area for their tactical decisions. Detailed knowledge of the acoustic propagation in this area will be a key to success in the prosecution of submarines and in the hunting of mines. Future tomography instruments may be dropped by maritime patrol aircraft to monitor an area of interest. Also, with the upcoming interest in low frequency active and bistatic sonars (Delmee et al., 1994), one can think of using their signals for acoustic tomography, thus providing an onboard capability to monitor the operational area of a task group. Requirements for moving ship tomography are within current technical possibilities. They include very accurate position- and timekeeping, already available through GPS. For coastal acoustic tomography though, we need a vertical hydrophone array as receiver since we have to spatially beamform as the temporal processing of the data is not sufficient to identify the different signal arrivals (Miller

et al., 1994). A vertical array is less easily usable from a surface vessel.

C. BARENTS SEA POLAR FRONT EXPERIMENT DATA

The Barents Sea Polar Front Experiment (BSPFEX), conducted by a team of the Naval Postgraduate School (NPS), Woods Hole Oceanographic Institution (WHOI) and Science Applications International Corporation (SAIC) in August 1992, is described by McLaughlin (1993). It provides this study with 159 two-dimensional tomography snapshots (Figure 3), with a five minutes interval, of a coastal, range varying environment. When these snapshots are used as sequential frames for a movie, we observe a wave motion in the SSP of the frontal system, adding the temporal variation of the SSP to the study with a resolution of 5 minutes. The spatial resolution of the sound speed data is 1000 meters in range and 2 meters in depth.

From these tomographic snapshots, the XBT data are extracted by using the SSP of one location, extrapolated over the whole area (Figure 4). We have chosen the location of the source for this study at position "23 km" in the tomographic slice to be also the location where the XBT is taken. The XBTs are taken at the beginning of the data sequence and at the synoptical hours 00.00 and 06.00 GMT. This establishes the temporal differences between the tomography snapshots and the XBT based calculations. By comparing Figures 3 and 4, we can expect a substantial difference for the acoustical conditions downslope of this location, towards the frontal system, while upslope the differences between the tomography and XBT data are more subtle.

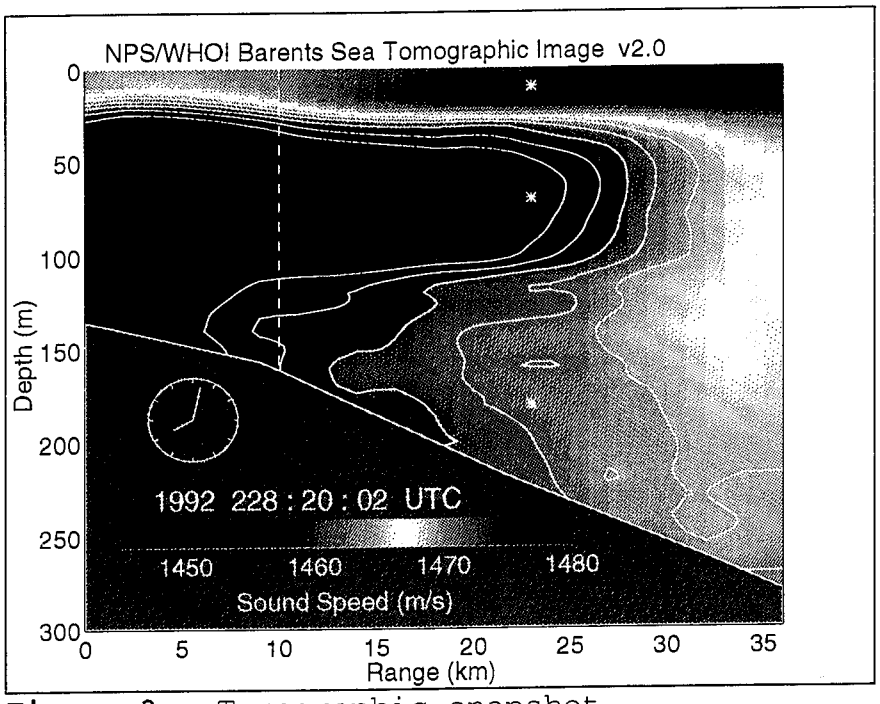

Figure 3. Tomographic snapshot.

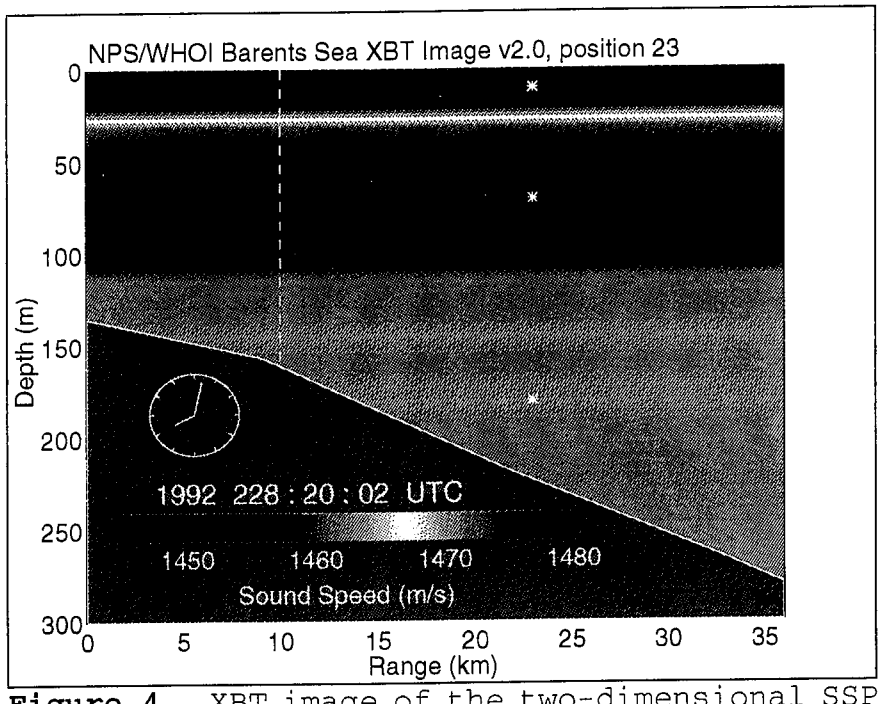

Figure 4. XBT image of the two-dimensional SSP derived from the tomographic snapshot.

At this location there are three different water masses to distinguish:

1. The warmer, shallow, mixed surface layer, extending to a depth of 20 meters.
2. The cold, Arctic water, sound channel between 20 and 120 meters depth.
3. The North Atlantic water layer at the bottom of the coastal ocean.

We studied three cases with the sonar lowered in one of above mentioned water masses. The used sonar depths are 10, 70 and 180 meter as indicated in Figures 3 and 4 by the "⊛." For this last sonar depth we keep a bottom clearance of 45 meters.

The bottom of the Barents Sea at this location consists of rock, covered by a 5 meter thick sediment. For the calculations we used the sound speeds and densities as displayed in Table 1.

The studied sonar range extended 13 kilometers up- and down slope from the sonar position as indicated in Figures 3 and 4 by the dashed line.

	sound speed (m/s)	density (kg/m^3)
water	i.a.w Figure 3	1026
sediment	1659	1830
bottom	4213	2600

Table 1. Sound speed and density data for the BSPFEX (sediment and bottom data obtained from US Naval Oceanographic Office: NAVOCEANO).

D. THE ENVIRONMENTAL ASSUMPTIONS

In order to calculate the transmission loss as a function of range and depth, we applied absorption to the pulse propagation. The absorption figures are derived from Clay and Medwin (1977). The modal attenuation coefficient is calculated for the frequency of 1000 Hz by the formula:

$$\alpha_n = \int_0^h \frac{1}{\rho(z)} Z_n^2(z)\,\alpha(z)\,dz \ , \qquad (1)$$

where $Z_n(z)$ is calculated by the normal mode code, α = 0.3 dB/m in the sediment and $\alpha = 8 \cdot 10^{-5}$dB/m in seawater. The depth of the waveguide, h in Equation (1), is for this study 300 meters.

Finally the modal attenuation coefficient is corrected for bottom and surface interactions. The coherent reflection coefficient for a surface having a Gaussian PDF is given by the following Equation (Clay and Medwin, 1977):

$$R_G = R e^{-2k^2\sigma^2\sin^2\theta_n} \ , \qquad (2)$$

where R = 1 for surface interactions and R = 0.759 for bottom interactions. For the Barents Sea σ = 0.25 meter for the bottom. For the surface we chose σ = 0.5 meter, corresponding with sea state 3. The bounce distance for each mode is calculated by (Chiu, 1994):

$$\Lambda_n = \frac{2\pi}{k_{n+1} - k_n} \ , \qquad (3)$$

with which the number of bounces for each mode over the range of 13 km is calculated.

For a source depth of 70 meters, these corrections contribute to the attenuation coefficient for mode 18 and higher modes. As shown in Figure 5, the attenuation for modes higher than 75 is larger than 0.5 Np/km. This is one reason to

limit the number of modes for the transmission loss calculations to 75.

For the probability of detection calculations we use a noise specrum level, NSL = 60 dB re 1μPa/Hz^{½}, as derived from the Wenz-curve (Kinsler et al., 1982) for sea state 3.

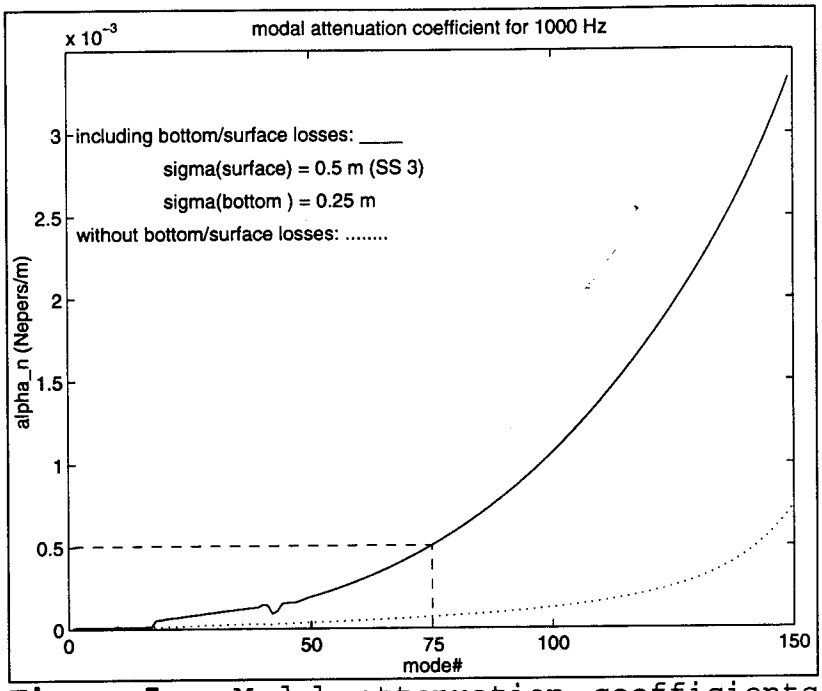

Figure 5. Modal attenuation coefficients for 1000 Hz.

III. THE HYPOTHETICAL SONAR SYSTEM

A. LOW FREQUENCY ACTIVE SONAR

Today's extremely quiet nuclear submarines as well as widespread conventional submarines are requiring many navies in the world to have research programs for low frequency active sonar systems. Threat scenarios have changed to area operations in coastal regions with a subsurface threat of very modern to old conventional submarines and of mines (O'Keefe, 1992). Current sonar systems do not provide sufficient detection capabilities in these scenarios. The submarines are too quiet for passive detection and their range advantage over ships fitted with hull mounted sonars is increasing.

A low frequency active sonar, with frequencies below 1000 Hz, can provide long range detection capabilities against quiet submarines, primarily in deep water. It can be designed monostatic, with source and receiver in one unit, or multistatic, with separate units for source and receivers. In confined and shallow waters a better option is an activated towed array sonar (ATAS), operating at slightly higher frequencies. Such a system by Thomson Sintra ASM and British Aerospace SEMA is currently on the market, operating at a frequency around 3 kHz (Jane's, 1994). The use of a low frequency active sonar in shallow water is under investigation (Delmee et al., 1994).

B. SONAR SYSTEM DESIGN FOR THIS STUDY

The bases of the sonar system design for this study are:

1. The experimental ALF sonar, designed by FEL-TNO in the Netherlands and built by Thomson Sintra ASM. The system is described by De Vlieger et al. (1994). Currently the Dutch Navy is testing the ALF in sea trials, planned from 1994 until 1997.

2. ATAS, designed and built by Thomson Sintra ASM and British Aerospace SEMA. The parameters are extracted from an undated sales brochure and Jane's (1994).

3. Suggestions of Directorate Material Royal Netherlands Navy, Department of Weapon and Communication Systems, division OSAO.

The system consists of a 1000 Hz towed source and, attached to the source body, a single receiver array. The design is similar to ATAS, using a hypothetical frequency. The parameters of the source are derived from the ALF sonar and shown in Table 2.

Frequency		1000 Hz
Source	acoustic power	1 kW
	horizontal beampattern	omni-directional
	vertical beamwidth	30°
	DI	4.5 dB
	SL	205.5 dB
	array dimensions	0.84x2.50 m
	# of transducers	2x6
	pulse	FM up-chirp
	pulse length	10 sec
	pulse swept bandwidth	100 Hz
Receiver	horizontal beamwidth	2°
	AG	15 dB
	array length	21.7 m
	# of hydrophones	32

Table 2. The hypothetical sonar system parameters.

1. The Source

The source consists of two vertical line arrays of six tonpilz transducers with a length of 2.5 meters as shown in Figure 6. It transmits a CW pulse at f = 1000 Hz with an acoustic power of 1 kW. For such a planar array, assuming no complex weighing, the elements to be omni-directional and for a speed of sound c = 1450 m/s, the far-field directivity function is:

$$D(f, f_x, f_z) = \sum_{m=0}^{1} \sum_{n=-2}^{3} e^{j2\pi((m-0.5) f_x dx + (n-0.5) f_z dz)} , \quad (4)$$

where:

$$f_x = \sin(\theta)\cos(\psi)\frac{f}{c} , \quad (5)$$

$$f_z = \cos(\theta)\frac{f}{c} \quad (6)$$

and the spacing between the elements dx=dz=42 cm. θ is the angle describing elevation and ψ represents the azimuthal angle. From the plot of the directivity function as shown in Figure 7, we can estimate the directivity index (Kinsler et al., 1982):

$$DI = 10\log_{10}\left(\frac{1}{\theta'}\right) , \quad (7)$$

where θ' is the -6dB half beam width in radians. The directivity index for the sonar, DI = 4.5 dB. The resulting source level, SL = 205.5 dB.

From the same figure, we measure the -3dB beamwidth to be 30°. To minimize the calculation time of the transmission loss calculations, we choose the half beamwidth to determine the maximum number of used normal modes. The angle of propagation

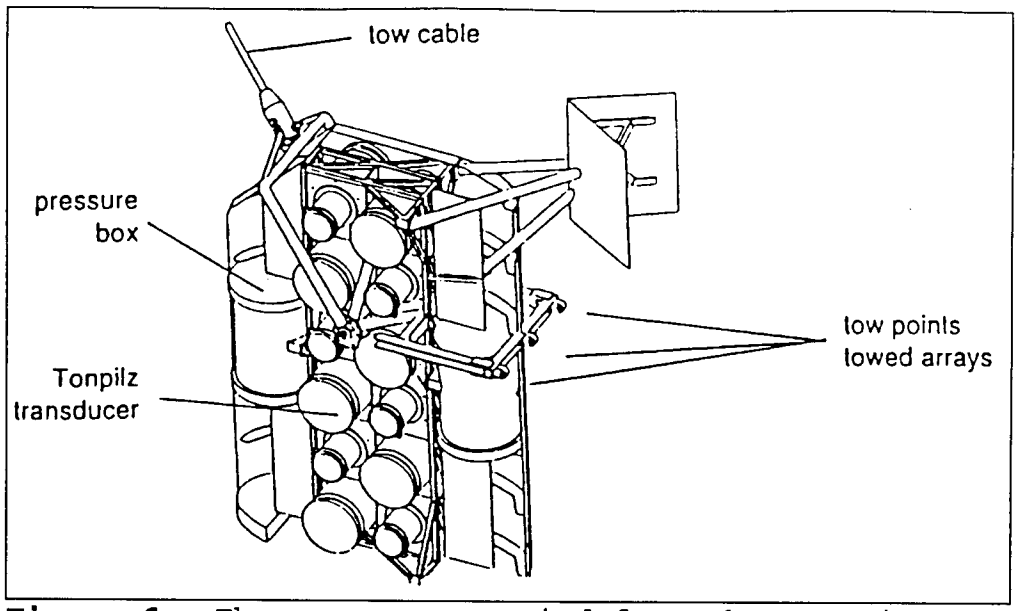

Figure 6. The source as copied from the experimental ALF sonar (De Vlieger et al., 1994).
(© Thomson Sintra ASM, reproduced by permission)

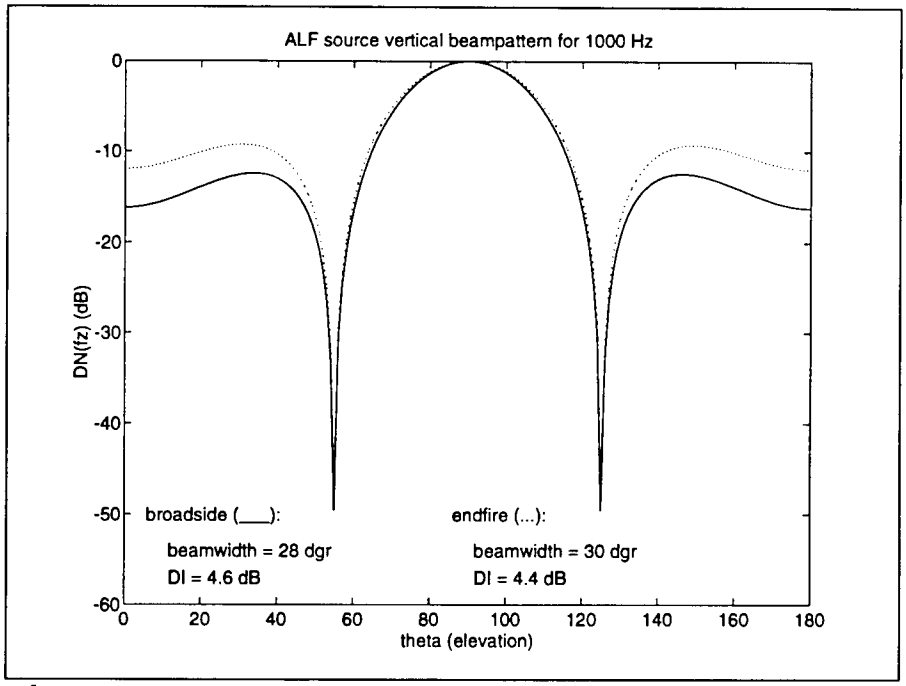

Figure 7. The directivity function for the hypothetical sonar source for a frequency of 1000 Hz.

of mode# 75, θ_n = 14.9°, thus providing a second reason to limit the calculations to 75 modes.

Use of low frequencies requires relative long pulses to meet a certain detection threshold. In order to have a reasonable range and doppler resolution, most low frequency active sonar systems will use frequency (FM) or phase (PM) modulated pulses. The hypothetical sonar system uses an up chirping, linear FM pulse with a 100 Hz swept bandwidth of length 10 seconds. But for the transmission loss calculations of this study, we modelled the source as a point source and limited the pulse to be a CW pulse at one frequency, again to minimize the computer calculation time.

2. The Receiver Array

The single receiver array with a length of 21.70 meters consists of 32 hydrophones with an elememt spacing of approximately half a wave length. It is towed behind the source as indicated in Figure 6. As shown in Figure 8, the broadside horizontal beamwidth is 2 degrees and the array gain, AG = 15 dB.

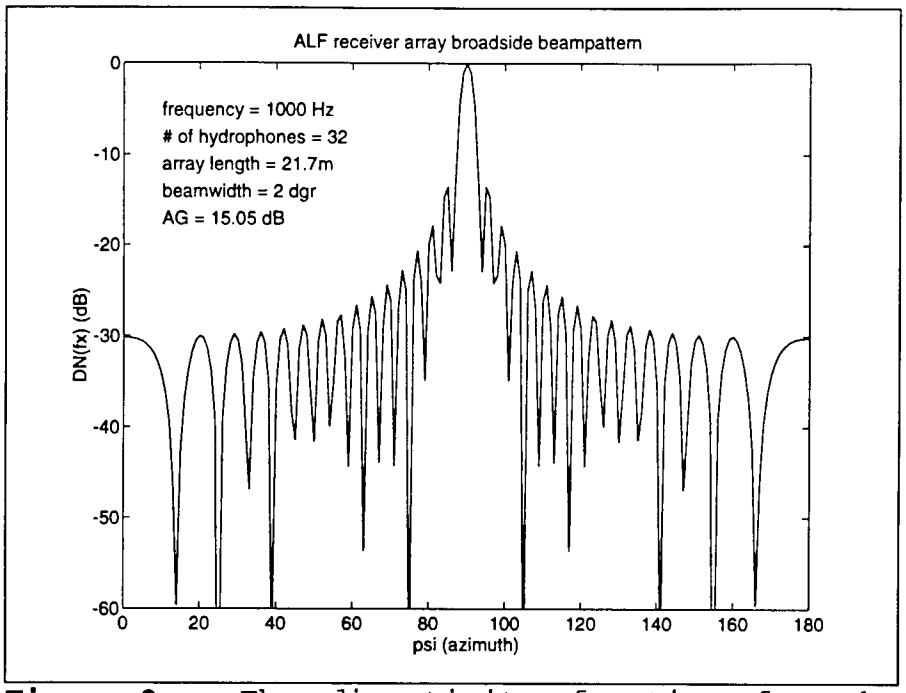

Figure 8. The directivity function for the hypothetical sonar receiver.

IV. THE TRANSMISSION LOSS CALCULATIONS

In order to assess the sonar performance in the ocean, we have to model the sound propagation through an inhomogeneous medium varying in four dimensions: three spatial variables and one time variable. In the imaged ocean of this study, the tomographic image, the soundspeed field varies in range, depth and time. We take care of the temporal fluctuations by calculating 159 sequential snapshots of the ocean with a 5 minutes spacing. Still the remaining two varying dimensions, range and depth, require a range dependent model for the sound propagation calculations. In case of shallow water and low frequency, a normal mode approach is suitable. Although for normal mode theory 1000 Hz is not considered to be a low frequency, the coupled normal mode model is particularly useful for active sonar applications (Chiu et al., 1994) as will be explained next.

A. COUPLED MODE APPROACH

The imaged ocean can be seen as a waveguide with significant environmental range variation; the SSP's are highly range dependent, especially across the front, and the bathymetry is varying. In such a case a travelling mode in the waveguide exchanges energy with other modes as explained by Chiu (1994). When it travels downslope over a gentle slope, the mode will exchange energy with the mode of one order lower. The modes are coupled. This requires a range dependent propagation model that calculates the propagating modes as a function of range.

The newly developed 3-D method we use in this study is a three-dimensional, broadband, coupled normal mode sound propagation model, described by Chiu et al. (1994) and provided to me by EOS Research Associates of Monterey, California. It assumes the ocean to be a linear, time-

invariant system that filters the input source signal and produces the output three-dimensional sound field. The model determines the ocean transfer function at various acoustic frequencies. To cut down in computation time we use a CW source at one frequency, 1000 Hz.

> For a given frequency, the basic formulation involves decomposing the acoustic pressure into slowly varying complex envelopes that modulate (mode by mode) analytic, rapidly-varying, adiabatic-mode solutions.... Since the formulation allows for sound speed and density to vary three-dimensionally and bathymetry to vary two-dimensionally, it is particular useful for...active sonar applications. (Chiu et al., 1994)

Modal attenuation coefficients are implemented to account for sound absorption in seawater and sediments, and boundary scattering (see Chapter II). Backscattering is neglected.

When only a small number of modes are required for the calculation, i.e. in shallow water and for low frequencies, the method is very effective. Since the frequency 1000 Hz stretched the model to its computational limits, we have reduced the number of used modes to 75 as justified in Chapter II and III. With the limitations imposed on the computations for this study, it takes on average $1^h08'$ per image to calculate the transmission loss for each frame, using a HP Apollo, series 735, workstation. While this is much longer than the 5 minutes interval between the subsequent tomographic data measurements, developments in computing hardware, software, and refinements in the propagation code could make this technique feasible in real time.

B. SET-UP OF THE TRANSMISSION LOSS COMPUTATIONS

We developed a code to calculate the transmission loss in a waveguide representing the imaged ocean of Figure 3. It sequentially calculates transmission loss for each snapshot,

including the XBT images at the beginning of the sequence and at the standard synoptical hours. We use the same coupled normal mode model to calculate the transmission loss for the tomographic and XBT snapshots. This implies that the calculations for the XBT snapshots are **not** range independent since the model takes the varying bathymetry into account. But this is the only fair methodology to compare both the tomographic and XBT images. Moreover the bathymetry data is normally available on board naval ships.

The computations are performed twice in a waveguide of depth 300 meters and length 13 kilometers: starting from the source, once downslope and once upslope as indicated in Figure 3. The input of the code consists of the source position in the imaged ocean and the sound speed and density fields in the water, sediment and bottom with a range increment of 1000 meters and a depth increment of 2 meters. For the computations as represented in this thesis, all other parameters to the coupled normal mode model are kept constant.

The broadband coupled normal mode model numerically integrates the differential equations governing the complex envelopes that describe the acoustic pressure, in the radial direction. To allow for economical computations, the range step size is automatically adjusted to the horizontal environmental variations. We choose the depth increment to be 0.75 meters, approximately half of the wavelength. This was the maximum possible depth step for calculations up to mode 75. Plots of the local normal modes showed aliasing effects for mode 100 and higher modes as can be seen in Figure 9f. Figures 9a-f show another interesting feature of the local normal modes close to the source. Low modes are more affected by the SSP while high modes are more affected by the bathymetry.

For each frequency, the code calculates the farfield sound pressure as a function of range, r, and depth, z:

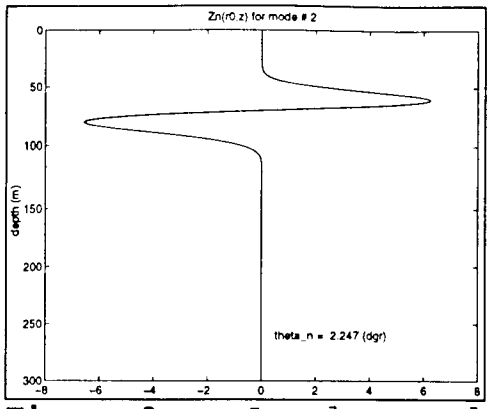

Figure 9a. Local normal mode for mode 2.

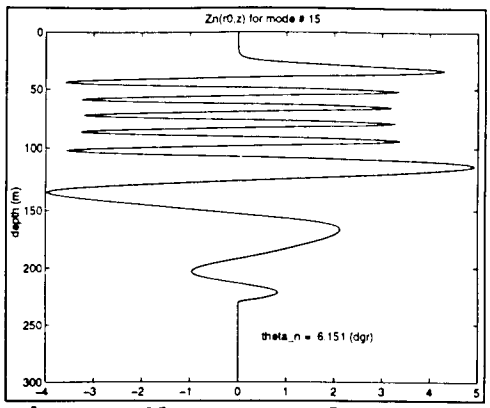

Figure 9b. Local normal mode for mode 15.

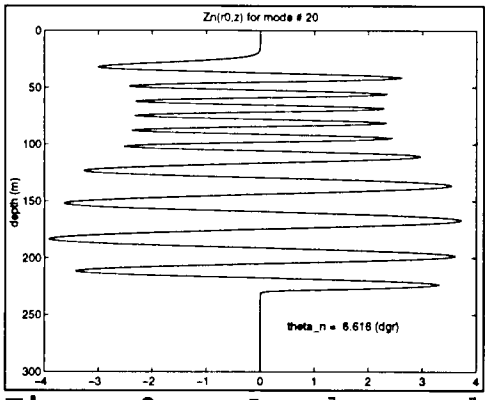

Figure 9c. Local normal mode for mode 20.

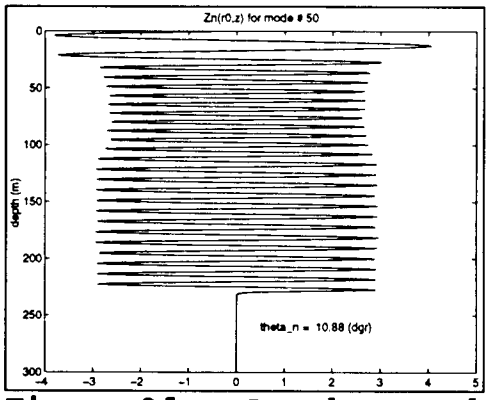

Figure 9d. Local normal mode for mode 50.

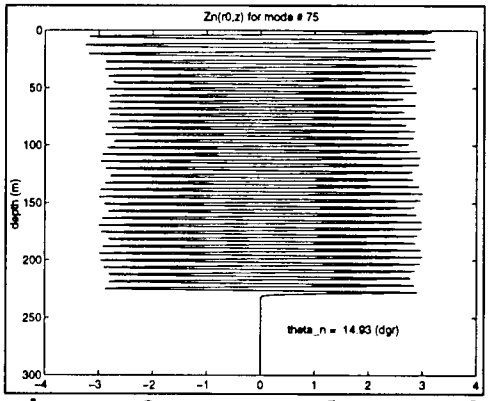

Figure 9e. Local normal mode for mode 75.

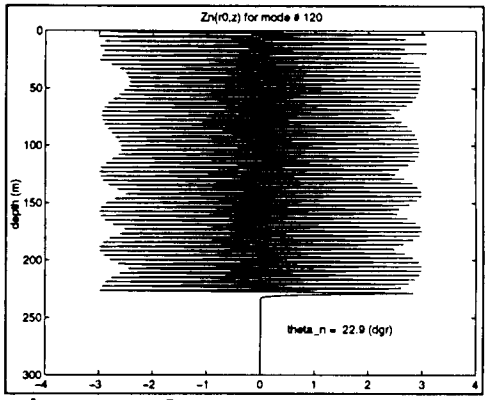

Figure 9f. Local normal mode for mode 120.

$$p(r,z) = \frac{P_0}{\sqrt{r}} \sum_{n=1}^{N} U_n(r)\, Z_n(z,r)\, e^{j\int_0^r k_n(r')\,dr'} , \qquad (8)$$

where P_0 is the rms pressure at 1 meter from the source, N is the number of propagating modes, U_n's are the slowly varying complex envelopes of the horizontal structure of the modes, Z_n's are the local normal modes and k_n's are the modal horizontal wave numbers. These variables are all given by the broadband coupled normal mode model. Hence the transmission loss, TL, can be calculated, using:

$$TL(r,z) = -10\log_{10}[p(r,z)\,p^*(r,z)] , \qquad (9)$$

where * denotes the complex conjugate. The acoustic pressure is a complex quantity since we include attenuation.

C. RESULTS

The output, the transmission loss, is plotted with a range increment of 500 meter and a depth increment of 2 meter. Two-hourly plots are shown in Appendices A, B and C for the respective source depth of 70, 180 and 10 meters. Additionally a movie of the 5-minute plots was made (Franken, 1994).

An example of the temporal transmission loss variations for a fixed position (range and depth) in the imaged ocean is shown in Figure 10. Besides the spatial difference in transmission loss between the tomographic and XBT calculations based on the choice of the location, Figure 10 shows clearly the temporal fluctuations of the tomography derived transmission loss. These fluctuations are wiped out for the XBT calculations since the XBT is only launched once every six hours.

In order to get a real flavor of the temporal transmission loss variations, it is more interesting to watch the movie mentioned above. While the movie of the SSP displays clearly a wave motion in the front of cold and warm water, the

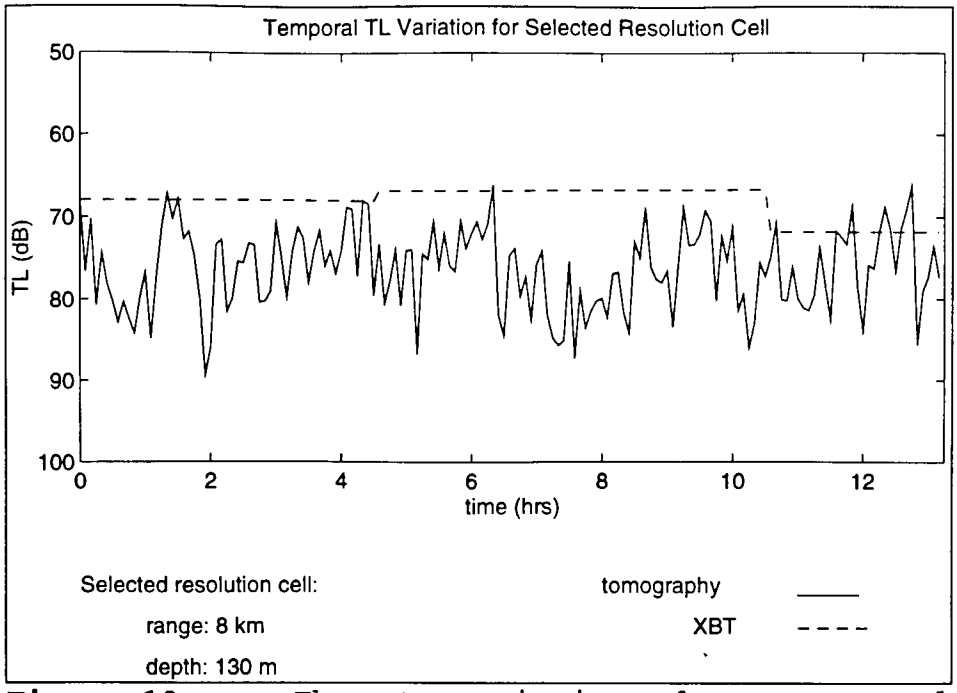

Figure 10. The transmission loss temporal variability at position: range 8 km downslope, depth 130 m.

transmission loss movie shows a more erratic behavior, especially downslope from the source towards the front. The transmission loss at a certain range from the source is affected cumulatively by all variations in the sound speed profiles between that range and the source. Many sound speed variations between source and field point makes the transmission loss vary randomly. Comparing subsequent snapshots, a temporal variation is clearly visible.

Comparing the XBT and tomography snapshots of the transmission loss, two obvious observations can be made.

1. In the tomographic snapshots the effects of the front are clearly visible: the energy of the sound refracts downward towards the bottom where the sound speed is the lowest. A spatial difference between the two snapshots in downslope direction can be observed.

2. Although the sound speed fields of the XBT and tomographic images do differ in range and time upslope from the source, the general structure of both sound fields remains the same and thus the transmission loss snapshots are similar. A spatial difference between the two snapshots in upslope direction is not clear.

These two observations are visualized in Figure 11. This Figure shows the mean difference in transmission loss between the tomographic and XBT calculations over the 159 available snapshots. The mean difference in transmission loss is calculated by the formula:

$$TL_{diff} = 10\log_{10}[<\frac{P_{Ti}^2}{P_{Xi}^2}>] \quad , \qquad \textbf{(10)}$$

where P_{Ti}^2 and P_{Xi}^2 are the acoustic intensities for the tomographic and XBT calculations respectively as a function of range and depth for snapshot "i."

We thus conclude that if the sound speed field does not change significantly in time and range, the XBT based transmission loss calculations and subsequent sonar assessment are similar to the tomographic snapshots. But in case of drastic sound speed field changes, in time or range, acoustic tomography will contribute a lot to a more accurate, range dependent transmission loss calculation. This is not only important in the case of this study, where a front changes the sound speed field drastically, but also for long range sonars in open ocean, where the sound speed structure of the sea changes gradually, but over a long distance from the source to its maximum range. It is also very important when temporal changes take place, unnoticed by the 6-hourly XBT, e.g. in case of a afternoon effect.

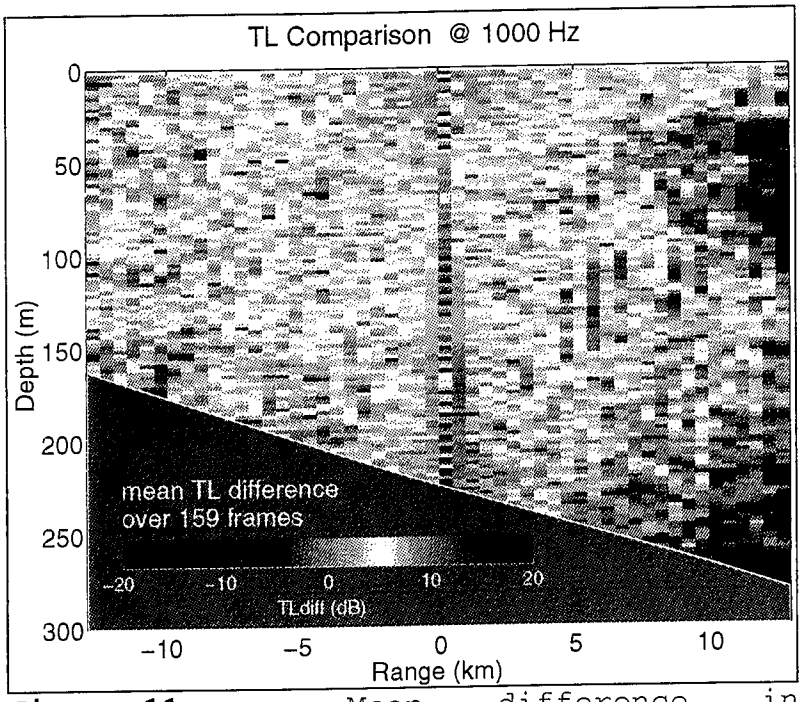

Figure 11. Mean difference in transmission loss between the tomographic and XBT calculations over 159 snapshots.

V. THE SONAR PERFORMANCE

An operational measure of sonar performance is the probability of detection. The probability of detection is defined as the probability of detecting a signal in the presence of noise, also called the single ping probability of detection or the glimpse probability. Clearly this is not the probability of target detection, since that may be a function of the probabilities for several pulses. Target detection depends also on many outside factors like relative movement of the target, sonar operator performance, etc. For sonar system performance assessment though, the single ping probability of detection is most appropriate. For the detection of the signal in the presence of noise we do not take any human factor of the sonar operator into account.

The single ping probability of detection can be derived using the concept of hypothesis testing as explained by Burdic (1984). Using the Neyman-Pearson criterion, we can express the probability of detection, P_D, as a function of the probability of false alarm and the signal-to-noise ratio (SNR) (Ziomek, 1985):

$$P_D = P_{fa}^{\frac{1}{1+SNR}} . \qquad (11)$$

The probability of false alarm used in this study, $P_{fa} = 10^{-4}$. The SNR is derived from the noise-limited (monostatic) active sonar Equation:

$$SNR(dB) = SL - 2TL + TS - NL + DI , \qquad (12)$$

where the source level, SL, is (Kinsler et al., 1982):

$$SL(re\,1\mu Pa) = 10\log\Pi + DI + 171 , \qquad (13)$$

for the acoustic power, Π = 1 kW, and the source directivity index, DI = 4.5 dB, as calculated in Equation (7). The

transmission loss, TL, is obtained by the coupled normal mode model. The target strength is a function of many target parameters and the frequency. A target strength, TS = 10 dB, is a reasonable assumption for a 60 meters long submarine, pinged abeam at 1 kHz (De Vlieger et al., 1994). The noise level, NL (see Chapter II), is calculated for the frequency bandwidth of 100 Hz. The directivity index, DI, in Equation (11) is the array gain, AG = $10\log_{10}(32 \text{ elem.})$ = 15 dB.

Equation (11) assumes noise limited conditions. We have not looked into reverberation limited conditions. This does not limit the research as long as we compare the tomographic and XBT snapshot under the same conditions.

Appendices A to C show the probability of detection for the source depths 70, 180 and 10 meters respectively. When the spatial and temporal variability of the ocean are large, in the downslope region from the source, there is a large difference in the probability of detection between the tomographic and XBT snapshots visible. Under these circumstances it is favorable to use tomography sound speed data for the sonar performance assessment.

VI. CONCLUSIONS

When the ocean sonar conditions vary significantly in range and time, a more realistic sonar performance assessment is to be expected using tomography sound speed data instead of XBT data. This becomes more important when long range sonars, such as low frequency active sonar, are involved. The ocean conditions are liable to change over the long maximum range of such a sonar system. This is also very important when temporal changes of the ocean conditions take place. An example of such a case besides the frontal system we use in this study, is the afternoon effect that can effect the performance of some sonars on a large scale.

The comparison between the sonar performance assessment using tomography data and XBT data is fair since we use the same model and assumptions for both. This study is limited though: we look only at the sonar performance in one scenario under noise limited conditions. The differentiation in source depth does not contribute much to the conclusions. For the source at 10 meter, the maximum sonar range is poor and thus the ocean conditions do not change significantly over this small range.

There will be a larger difference between the XBT SSP derived from tomographic measurements and from a real XBT-reading than assumed in this study. The sound speed does not solely depend on the ocean temperature, thus introducing a systematic error in the XBT derived sound speed data. This can be avoided by using an XSV measurement.

Comparing the transmission loss computer computation time ($1^h08'$) and the temporal resolution of the tomography snapshots (5 minutes), it is clear that the sonar performance assessment for this 1000 Hz sonar using this broadband, coupled normal mode model, can not be performed real time. Though for lower frequencies, requiring less normal modes for

the calculations, the computer computation time decreases manifold.

The trend of lower and lower the frequency of active sonars for future anti-submarine warfare and the increasing interest in deploying ASW assets in littoral waters, both require knowledge of the sound speed field in the area of operation with high spatial and temporal resolutions. Low frequency, long range sonars deal with spatial varying ocean conditions. Shallow, coastal waters are liable for large spatial and temporal variations in their sound speed fields. Acoustic tomography is the only efficient technique that provides sufficiently detailed sound speed data for range dependent propagation models to calculate the performance assessment of future sonars. Moreover the use of the same very low frequency active sonars for on board, moving ship tomography lies within current technological capabilities.

LIST OF REFERENCES

Burdic, W.S., *Underwater Acoustic System Analysis*, Prentice-Hall, Inc., Englewood Cliffs, NJ, 1984.

Chiu, C.-S., *Downslope Modal Energy Conversion*, JASA 95(3), March 1994.

Chiu, C.-S., Miller, J.H., Denner, W.W., and Lynch, J.F., *A Three-Dimensional, Broadband, Coupled Normal-Mode Sound Propagation Modeling Approach*, in **Full Field Inversion Methods in Ocean and Seismic Acoustics**, eds. Diachok, O., Caiti, A., Gerstoft, P., and Schmidt, H., Kluwer Academic Publishers, 1994.

Clay, C.S., Medwin, H., *Acoustical Oceanography: Principles and Applications*, John Wiley & Sons, New York, 1977.

Delmee, M.H.M., Dongen, M.P.F.M. van, and Verschelling, M., *Actief Laag Frequent sonar: het antwoord op een dreiging van stiller wordende onderzeeboten?(1)*, Marineblad (KVMO, Royal Netherlands Naval Officer's Association), February 1994.

Franken, J., *A Tactical Application of Coastal Acoustic Tomography*, video made at the Naval Postgraduate School, November 1994.

Jane's, *Underwater Warfare Systems 1994-1995*, ed. Watts, A.J., sixth edition, Jane's Information Group Inc., Coulsdon (UK), 1994.

Kinsler, L.E., Frey, A.R., Coppens, A.B. and Sanders, J.V., *Fundamentals of Acoustics*, third edition, John Wiley & Sons, New York, 1982.

McLaughlin, P.G., *Signal Processing for the 1992 Barents Sea Tomography Experiment*, MS Thesis, Naval Postgraduate School, December 1993.

Miller, J.H., Chiu, C.-S. and Lynch, J.F., *Signal Processing for Coastal Acoustic Tomography*, in **Environmental Acoustics**, eds. Lee, D. and Schultz, M., World Scientific, Singapore, 1994.

Miller, J.H. and Franken, J., *Ocean Acoustic Tomography*, Marineblad (KVMO, Royal Netherlands Naval Officer's Association), November 1994.

Munk, W. and Wunsch, C., *Ocean Acoustic Tomography: a Scheme for Large Scale Monitoring*, Deep-Sea Research 26A, pp. 123-161, 1979.

O'Keefe, S., Kelso II, F.B., Mundy, C.E., *...From the Sea: Preparing the Naval Service for the 21st Century*, Naval Institute Proceedings, November 1992.

Spindel, R.C. and Worcester, P.F., *Ocean Acoustic Tomography*, Scientific American, October 1990.

Vlieger, J.H. de, Ballegooijen, E.C. van, and Kreijger, J.B., *Actief Laag Frequent sonar: het antwoord op een dreiging van stiller wordende onderzeeboten?(2)*, Marineblad (KVMO, Royal Netherlands Naval Officer's Association), March 1994.

Ziomek, L.J., *Underwater Acoustics: a Linear Systems Theory Approach*, Academic Press, Inc., San Diego, CA, 1985.

APPENDIX A. TL AND POD ESTIMATES FOR SOURCE DEPTH 70 METER

This Appendix contains the figures of the transmission loss and probability of detection estimates for the source at a depth of 70 meters. The figures are represented at two-hour intervals. The XBT data is derived from the tomography data at the beginning of the sequence (Figure 3) and at six-hour intervals, starting at midnight.

These same figures, separated by five minute time intervals, are used as frames for a movie. The movie shows clearly the variability of the ocean and the resulting eratic variations of the transmission loss and probability of detection.

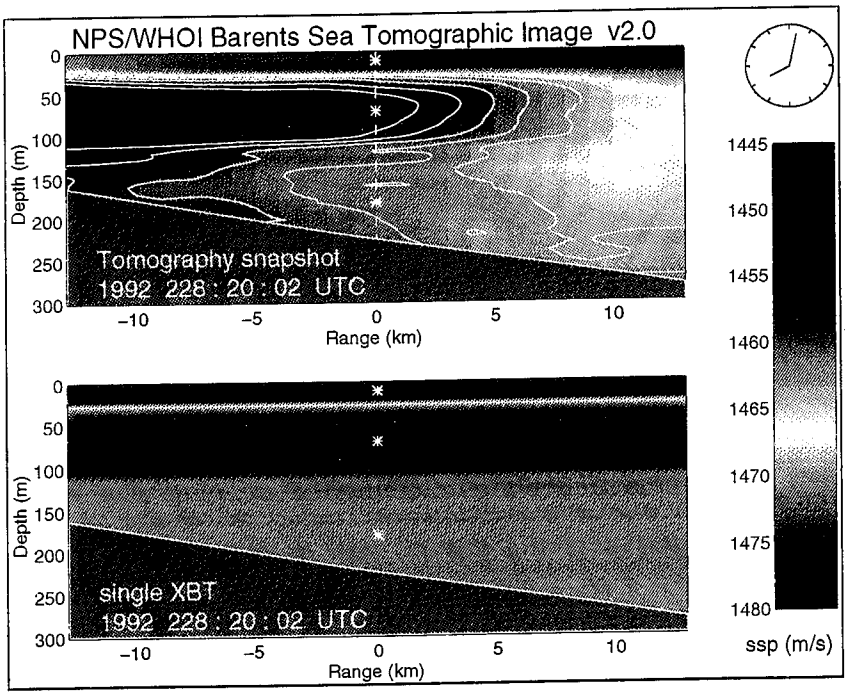

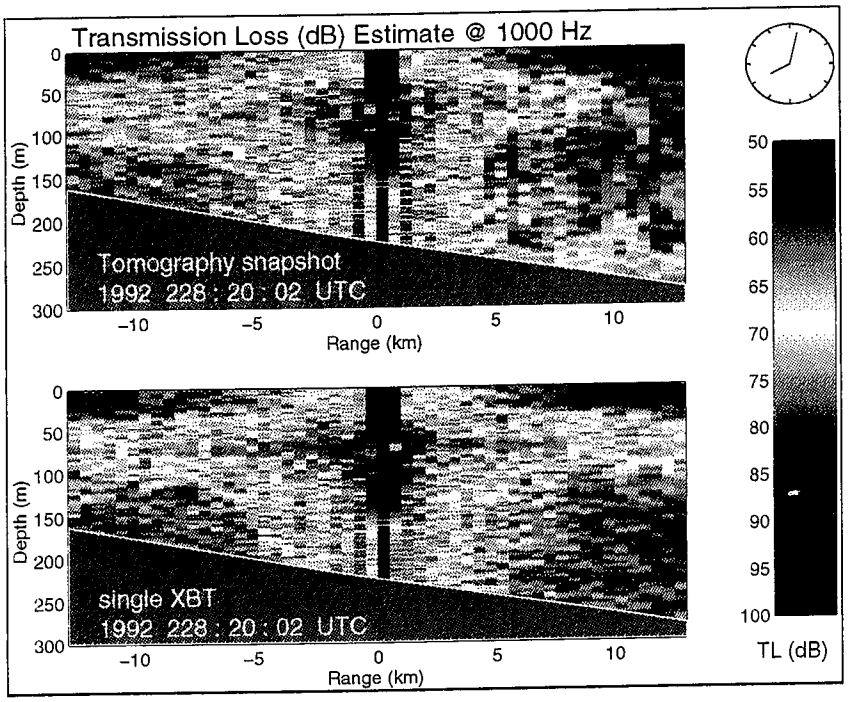
Transmission Loss (dB) Estimate @ 1000 Hz
Depth (m)
Tomography snapshot
1992 228 : 20 : 02 UTC
Range (km)
single XBT
1992 228 : 20 : 02 UTC
Range (km)
TL (dB)

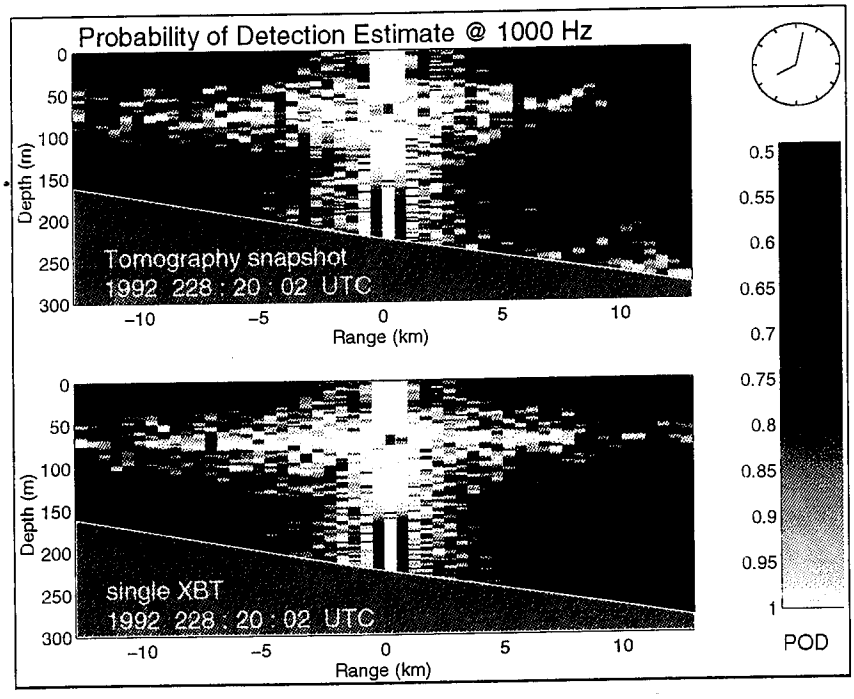
Probability of Detection Estimate @ 1000 Hz
Depth (m)
Tomography snapshot
1992 228 : 20 : 02 UTC
Range (km)
single XBT
1992 228 : 20 : 02 UTC
Range (km)
POD

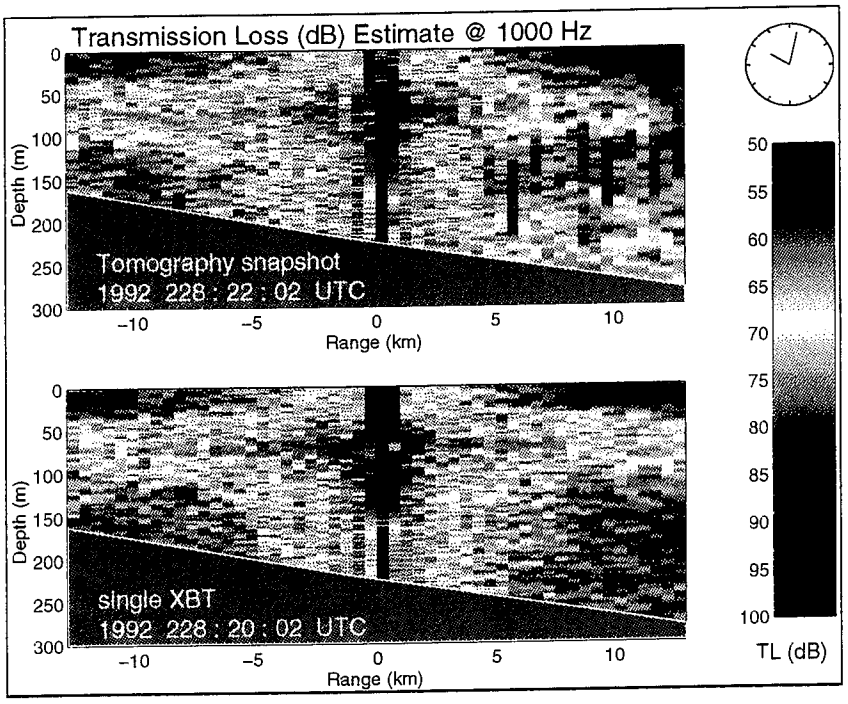
Transmission Loss (dB) Estimate @ 1000 Hz
Depth (m)
Tomography snapshot
1992 228 : 22 : 02 UTC
Range (km)
single XBT
1992 228 : 20 : 02 UTC
TL (dB)

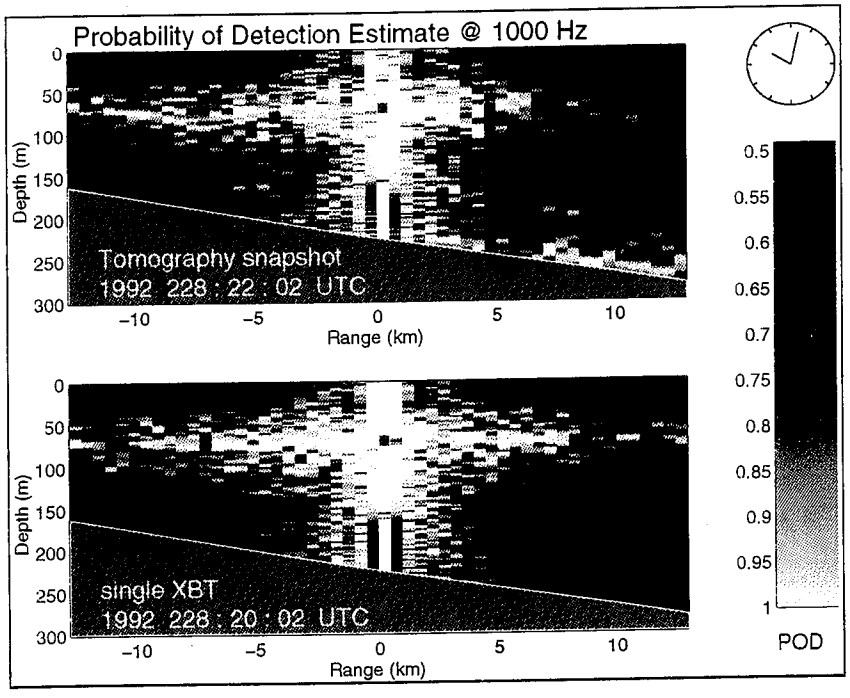
Probability of Detection Estimate @ 1000 Hz
Depth (m)
Tomography snapshot
1992 228 : 22 : 02 UTC
Range (km)
single XBT
1992 228 : 20 : 02 UTC
POD

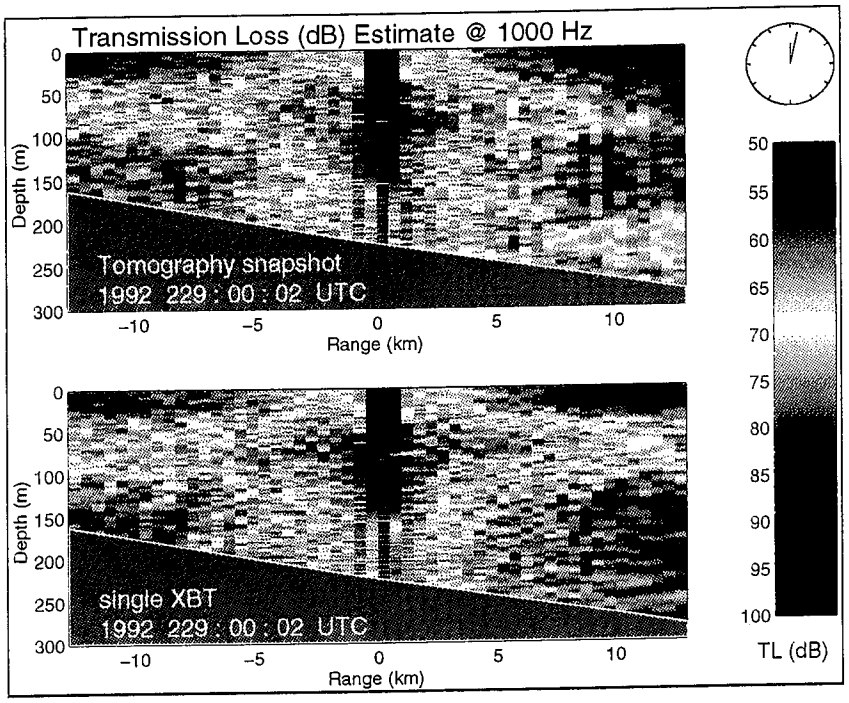
Transmission Loss (dB) Estimate @ 1000 Hz
Depth (m)
0
50
100
150
200
250
300
Tomography snapshot
1992 229 : 00 : 02 UTC
−10
−5
0
5
10
Range (km)
single XBT
1992 229 : 00 : 02 UTC
50
55
60
65
70
75
80
85
90
95
100
TL (dB)

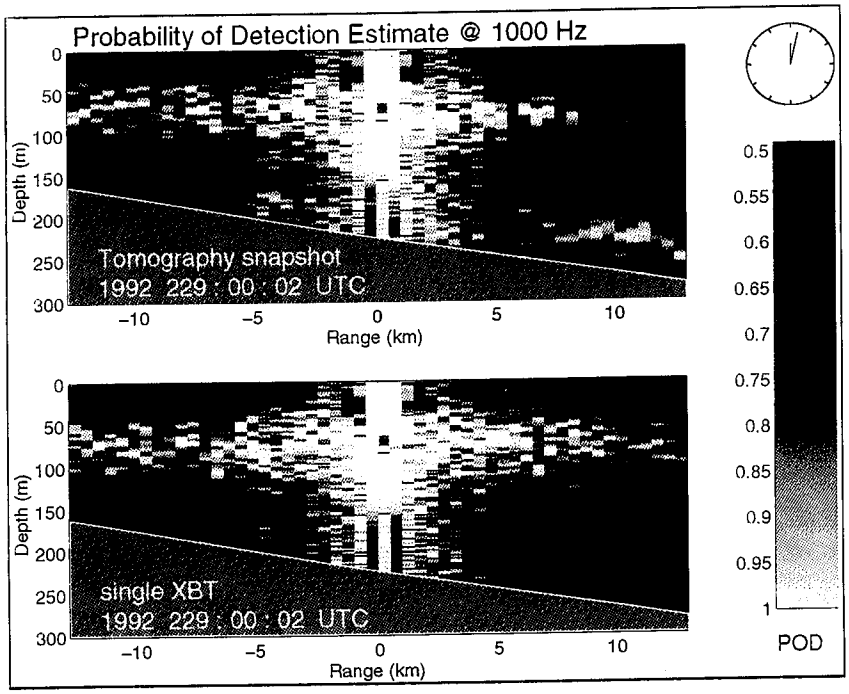
Probability of Detection Estimate @ 1000 Hz
Depth (m)
0
50
100
150
200
250
300
Tomography snapshot
1992 229 : 00 : 02 UTC
−10
−5
0
5
10
Range (km)
single XBT
1992 229 : 00 : 02 UTC
0.5
0.55
0.6
0.65
0.7
0.75
0.8
0.85
0.9
0.95
1
POD

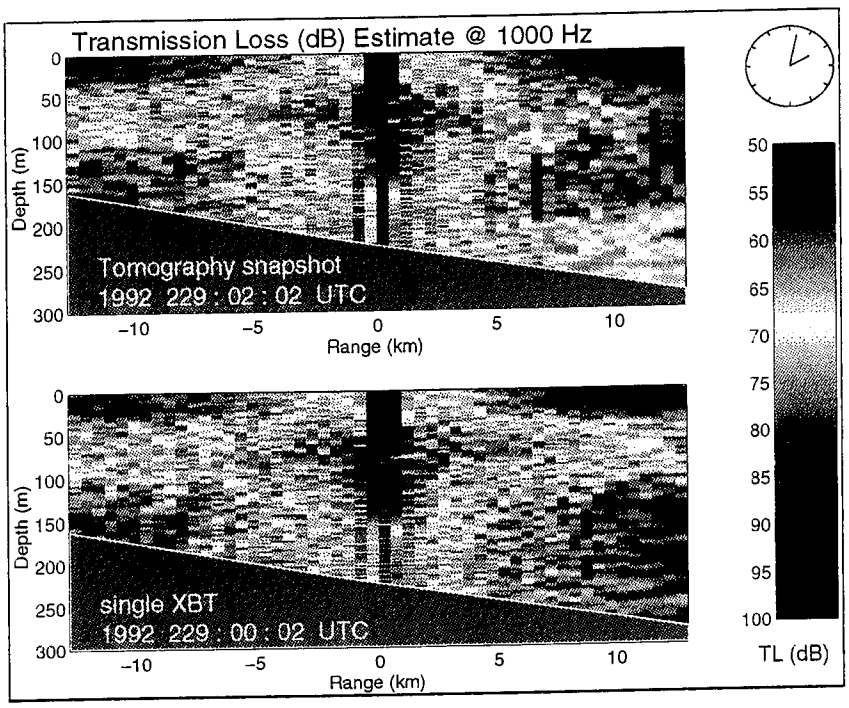
Transmission Loss (dB) Estimate @ 1000 Hz
Depth (m)
0
50
100
150
200
250
300
Tomography snapshot
1992 229 : 02 : 02 UTC
−10
−5
0
5
10
Range (km)
single XBT
1992 229 : 00 : 02 UTC
50
55
60
65
70
75
80
85
90
95
100
TL (dB)

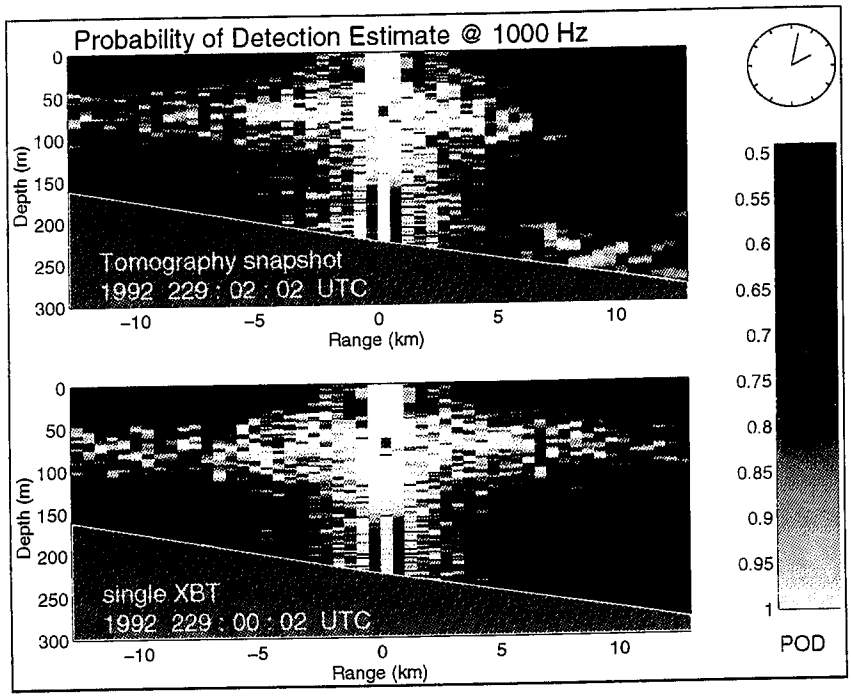
Probability of Detection Estimate @ 1000 Hz
Depth (m)
0
50
100
150
200
250
300
Tomography snapshot
1992 229 : 02 : 02 UTC
−10
−5
0
5
10
Range (km)
single XBT
1992 229 : 00 : 02 UTC
0.5
0.55
0.6
0.65
0.7
0.75
0.8
0.85
0.9
0.95
1
POD

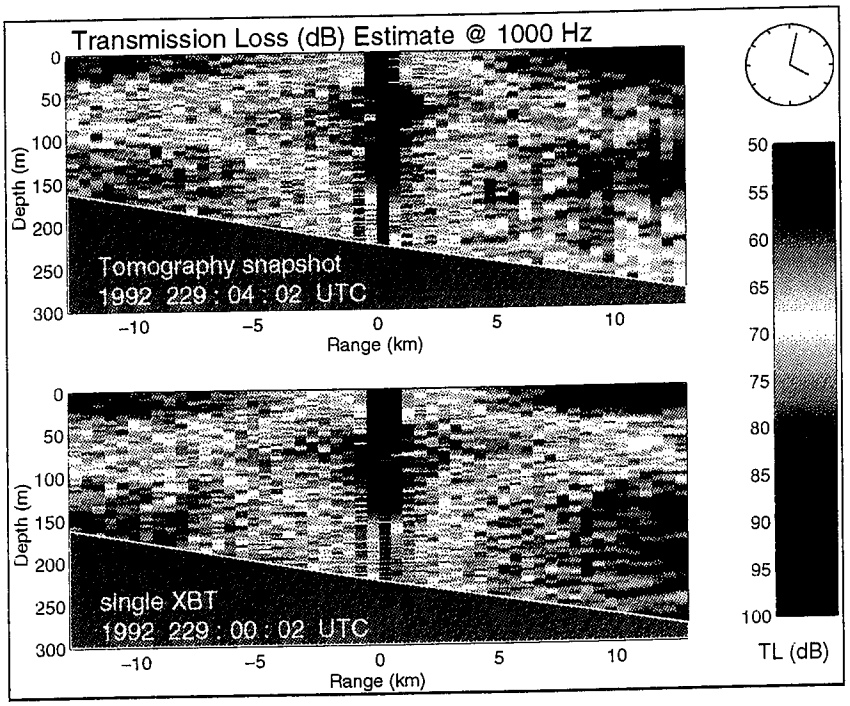
Transmission Loss (dB) Estimate @ 1000 Hz
Depth (m)
0
50
100
150
200
250
300
Tomography snapshot
1992 229 : 04 : 02 UTC
−10
−5
0
5
10
Range (km)
single XBT
1992 229 : 00 : 02 UTC
50
55
60
65
70
75
80
85
90
95
100
TL (dB)

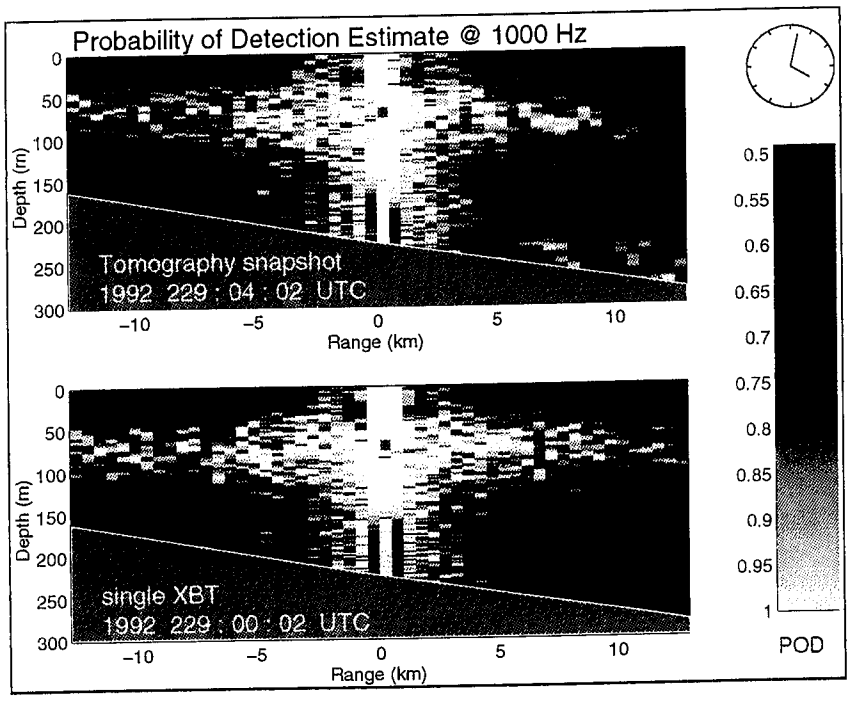
Probability of Detection Estimate @ 1000 Hz
Depth (m)
0
50
100
150
200
250
300
Tomography snapshot
1992 229 : 04 : 02 UTC
−10
−5
0
5
10
Range (km)
single XBT
1992 229 : 00 : 02 UTC
0.5
0.55
0.6
0.65
0.7
0.75
0.8
0.85
0.9
0.95
1
POD

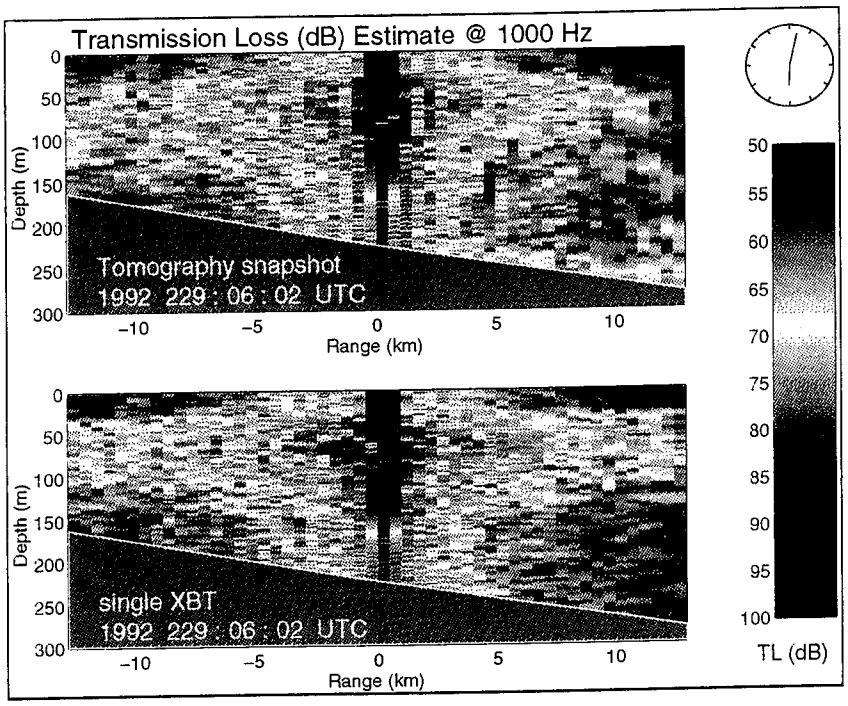
Transmission Loss (dB) Estimate @ 1000 Hz
Depth (m)
0
50
100
150
200
250
300
Tomography snapshot
1992 229 : 06 : 02 UTC
−10
−5
0
5
10
Range (km)
single XBT
1992 229 : 06 : 02 UTC
50
55
60
65
70
75
80
85
90
95
100
TL (dB)

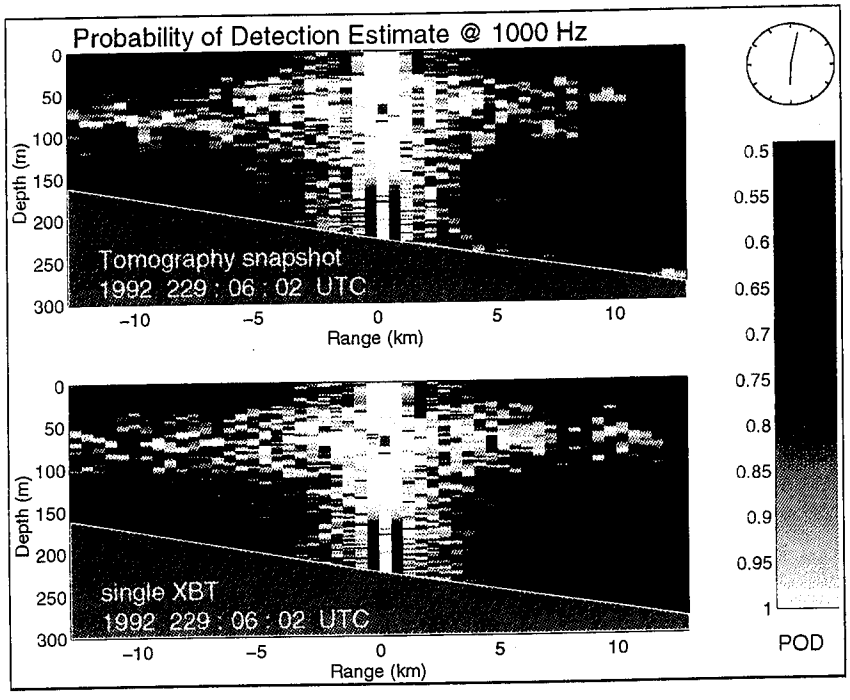
Probability of Detection Estimate @ 1000 Hz
Depth (m)
0
50
100
150
200
250
300
Tomography snapshot
1992 229 : 06 : 02 UTC
−10
−5
0
5
10
Range (km)
single XBT
1992 229 : 06 : 02 UTC
0.5
0.55
0.6
0.65
0.7
0.75
0.8
0.85
0.9
0.95
1
POD

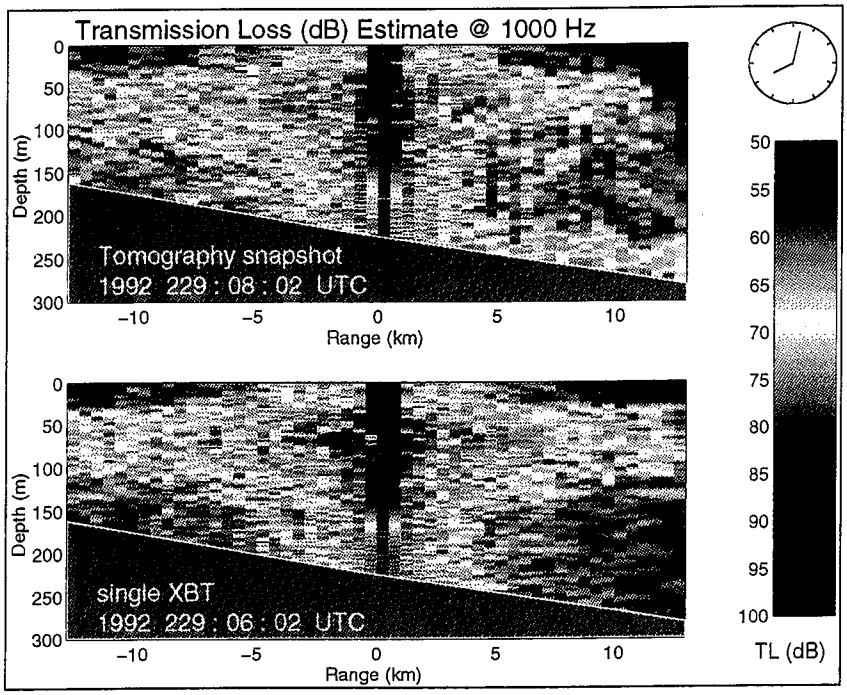
Transmission Loss (dB) Estimate @ 1000 Hz
Depth (m)
Tomography snapshot
1992 229 : 08 : 02 UTC
Range (km)
single XBT
1992 229 : 06 : 02 UTC
TL (dB)

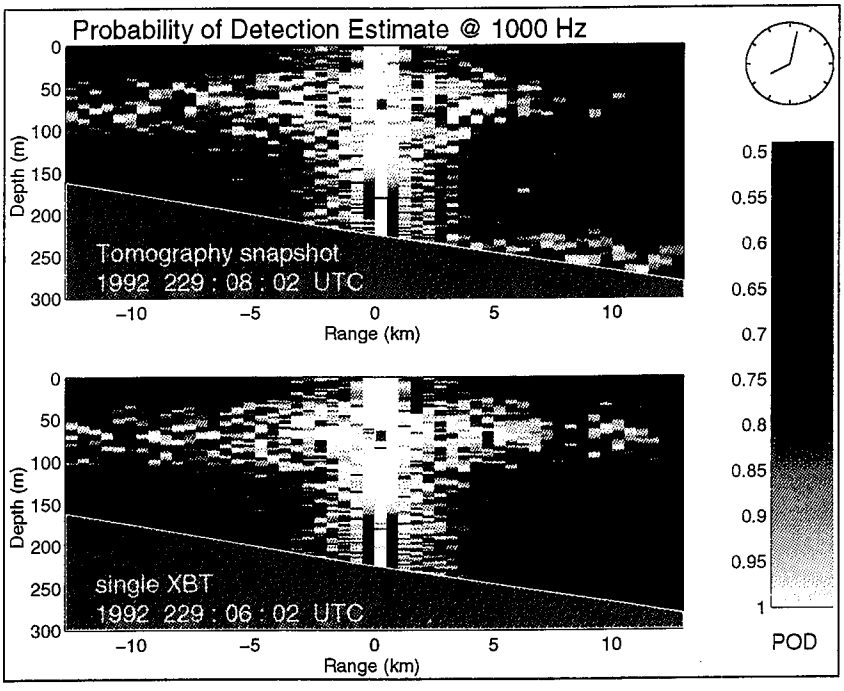
Probability of Detection Estimate @ 1000 Hz
Depth (m)
Tomography snapshot
1992 229 : 08 : 02 UTC
Range (km)
single XBT
1992 229 : 06 : 02 UTC
POD

APPENDIX B. TL AND POD ESTIMATES FOR SOURCE DEPTH 180 METER

This Appendix contains the figures of the transmission loss and probability of detection estimates for the source at a depth of 180 meters. The figures are represented at two-hour intervals. The XBT data is derived from the tomography data at the beginning of the sequence (Figure 3) and at six-hour intervals, starting at midnight.

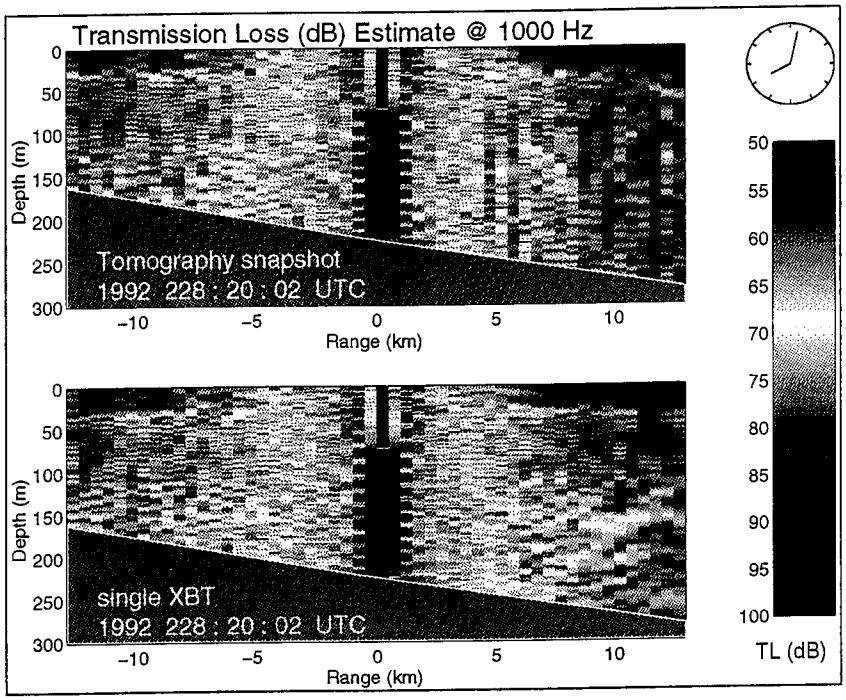
Transmission Loss (dB) Estimate @ 1000 Hz
Depth (m)
0
50
100
150
200
250
300
Tomography snapshot
1992 228 : 20 : 02 UTC
−10
−5
0
5
10
Range (km)
single XBT
1992 228 : 20 : 02 UTC
50
55
60
65
70
75
80
85
90
95
100
TL (dB)

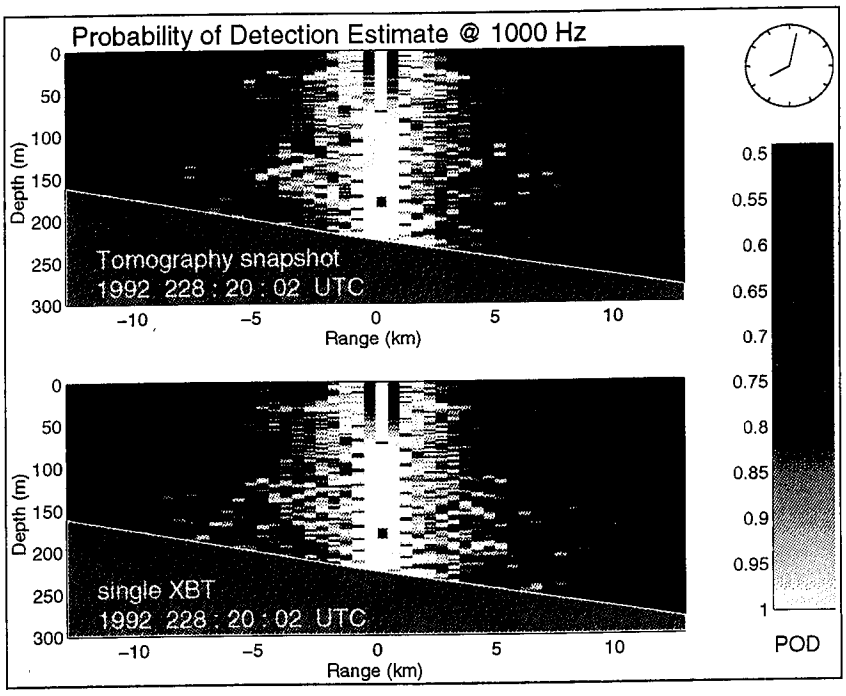
Probability of Detection Estimate @ 1000 Hz
Depth (m)
0
50
100
150
200
250
300
Tomography snapshot
1992 228 : 20 : 02 UTC
−10
−5
0
5
10
Range (km)
single XBT
1992 228 : 20 : 02 UTC
0.5
0.55
0.6
0.65
0.7
0.75
0.8
0.85
0.9
0.95
1
POD

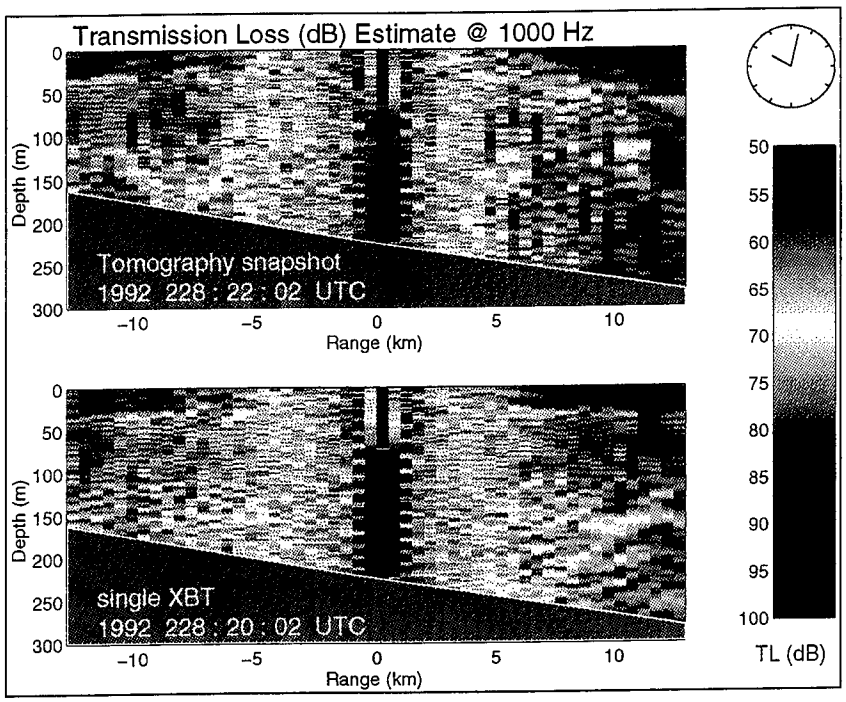
Transmission Loss (dB) Estimate @ 1000 Hz
Depth (m)
0
50
100
150
200
250
300
Tomography snapshot
1992 228 : 22 : 02 UTC
−10
−5
0
5
10
Range (km)
single XBT
1992 228 : 20 : 02 UTC
50
55
60
65
70
75
80
85
90
95
100
TL (dB)

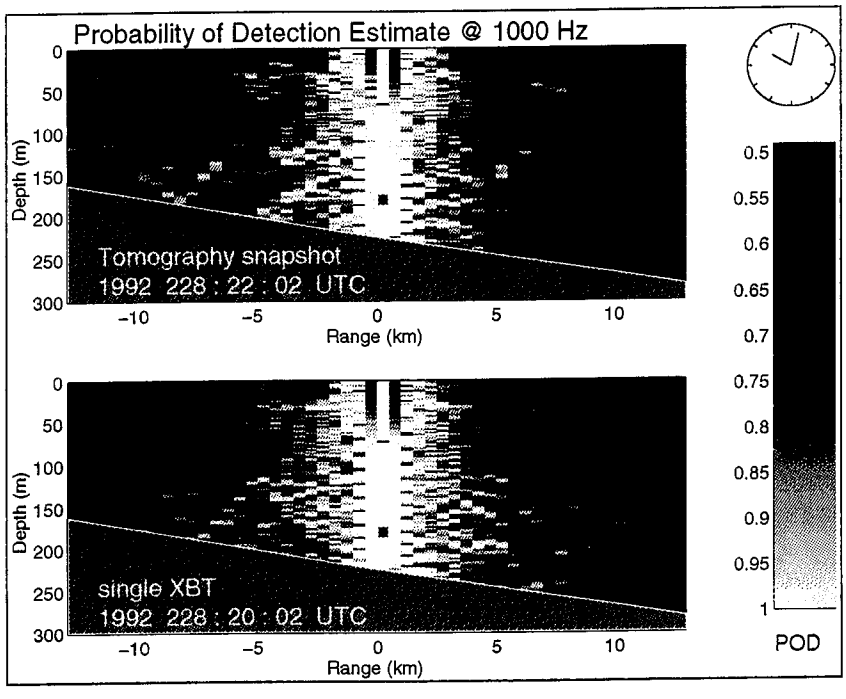
Probability of Detection Estimate @ 1000 Hz
Depth (m)
0
50
100
150
200
250
300
Tomography snapshot
1992 228 : 22 : 02 UTC
−10
−5
0
5
10
Range (km)
single XBT
1992 228 : 20 : 02 UTC
0.5
0.55
0.6
0.65
0.7
0.75
0.8
0.85
0.9
0.95
1
POD

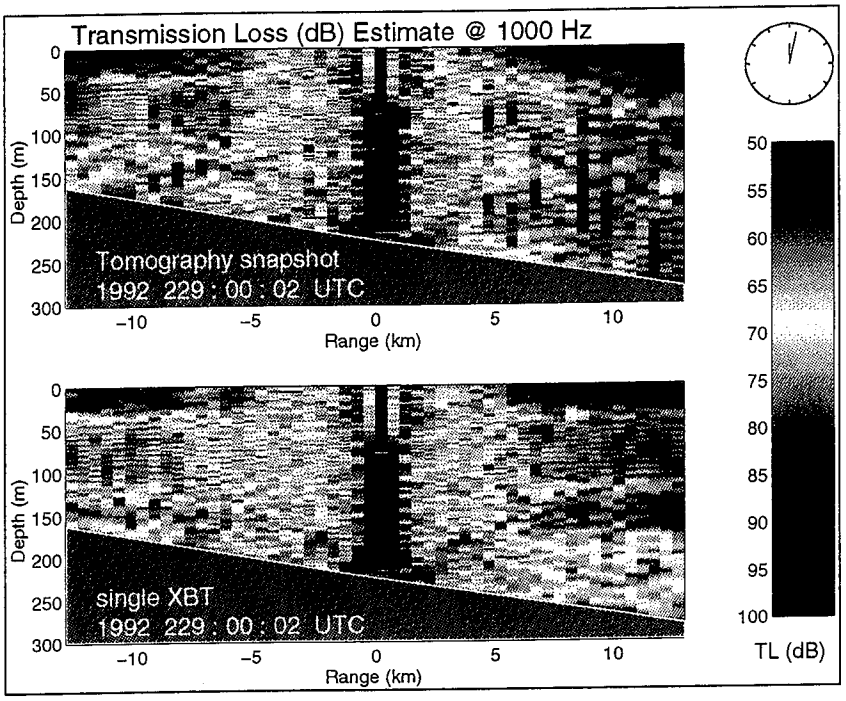
Transmission Loss (dB) Estimate @ 1000 Hz
Depth (m)
0
50
100
150
200
250
300
Tomography snapshot
1992 229 : 00 : 02 UTC
−10
−5
0
5
10
Range (km)
single XBT
1992 229 : 00 : 02 UTC
50
55
60
65
70
75
80
85
90
95
100
TL (dB)

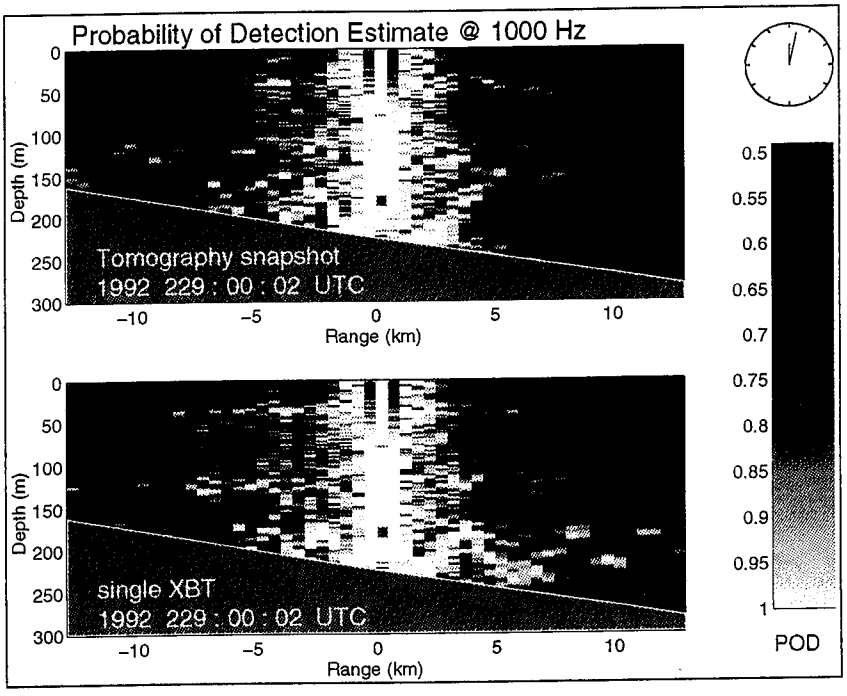
Probability of Detection Estimate @ 1000 Hz
Depth (m)
0
50
100
150
200
250
300
Tomography snapshot
1992 229 : 00 : 02 UTC
−10
−5
0
5
10
Range (km)
single XBT
1992 229 : 00 : 02 UTC
0.5
0.55
0.6
0.65
0.7
0.75
0.8
0.85
0.9
0.95
1
POD

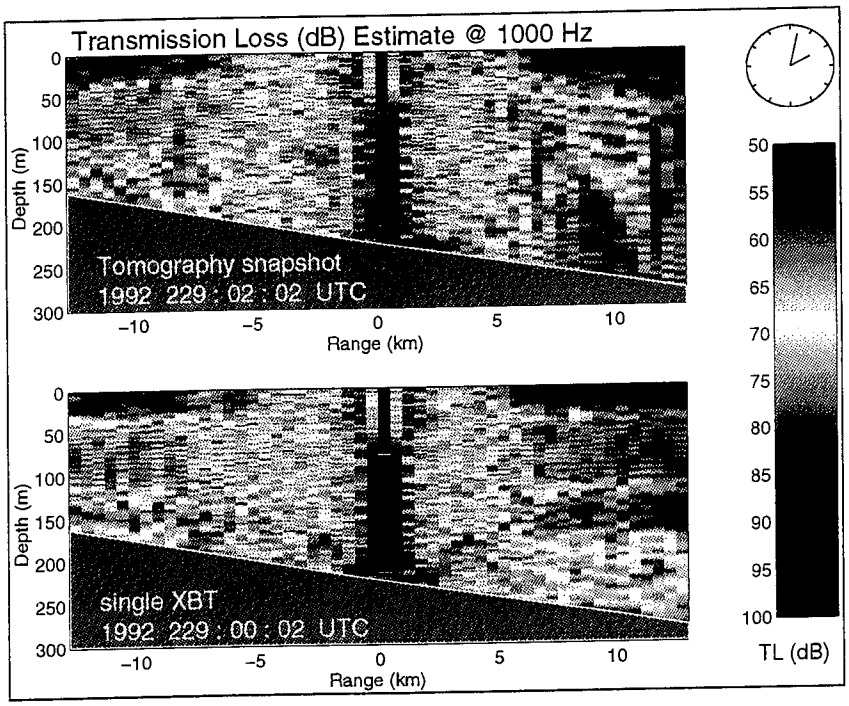
Transmission Loss (dB) Estimate @ 1000 Hz
Depth (m)
Tomography snapshot
1992 229 : 02 : 02 UTC
Range (km)
single XBT
1992 229 : 00 : 02 UTC
Range (km)
TL (dB)

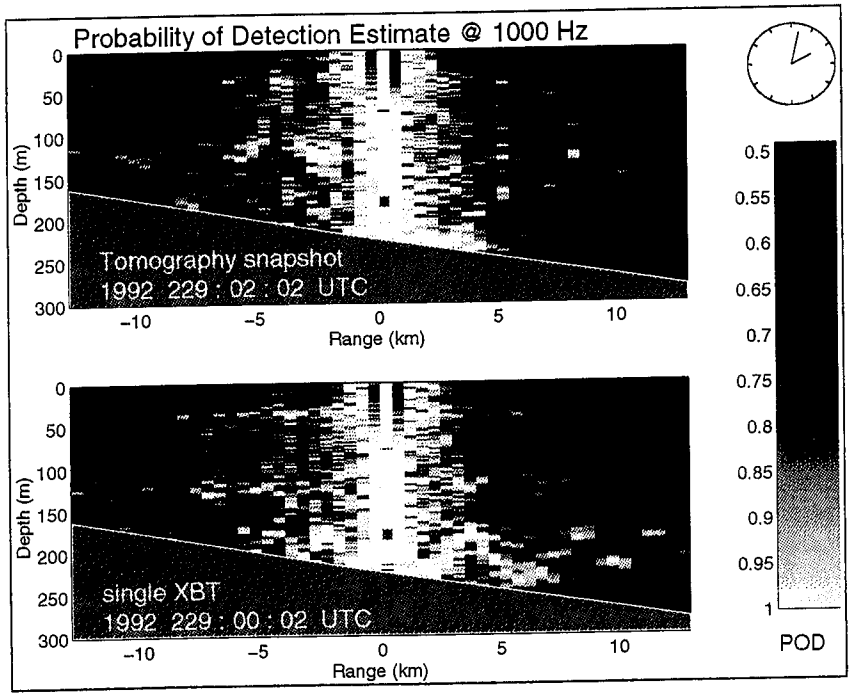
Probability of Detection Estimate @ 1000 Hz
Depth (m)
Tomography snapshot
1992 229 : 02 : 02 UTC
Range (km)
single XBT
1992 229 : 00 : 02 UTC
Range (km)
POD

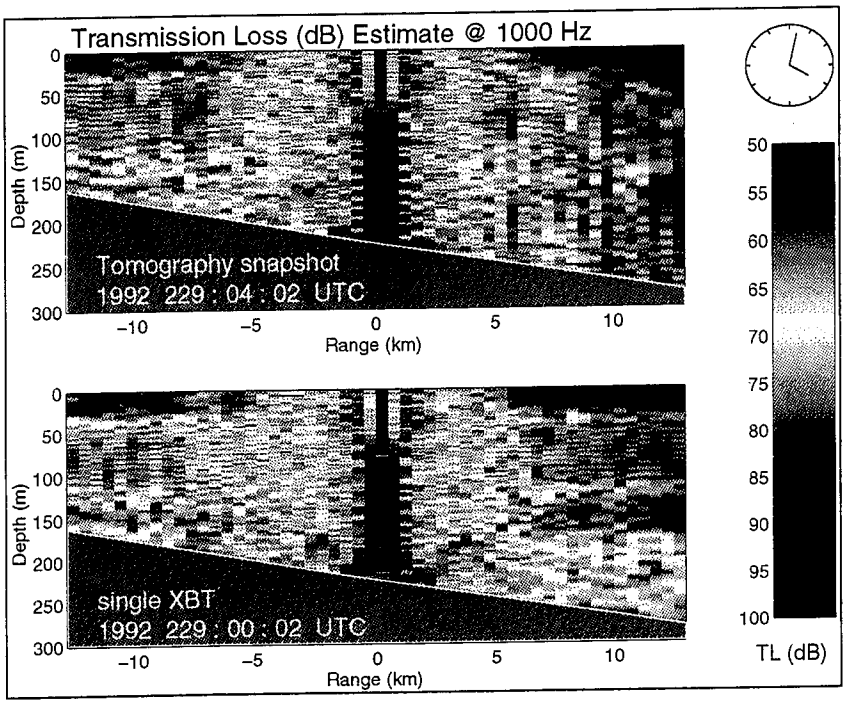
Transmission Loss (dB) Estimate @ 1000 Hz
Depth (m)
0
50
100
150
200
250
300
Tomography snapshot
1992 229 : 04 : 02 UTC
−10
−5
0
5
10
Range (km)
single XBT
1992 229 : 00 : 02 UTC
50
55
60
65
70
75
80
85
90
95
100
TL (dB)

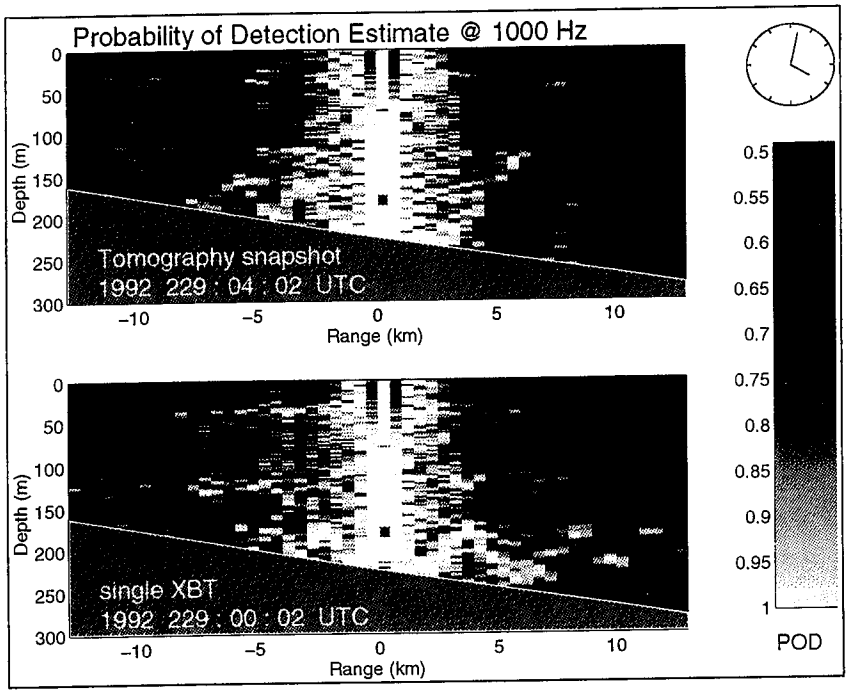
Probability of Detection Estimate @ 1000 Hz
Depth (m)
0
50
100
150
200
250
300
Tomography snapshot
1992 229 : 04 : 02 UTC
−10
−5
0
5
10
Range (km)
single XBT
1992 229 : 00 : 02 UTC
0.5
0.55
0.6
0.65
0.7
0.75
0.8
0.85
0.9
0.95
1
POD

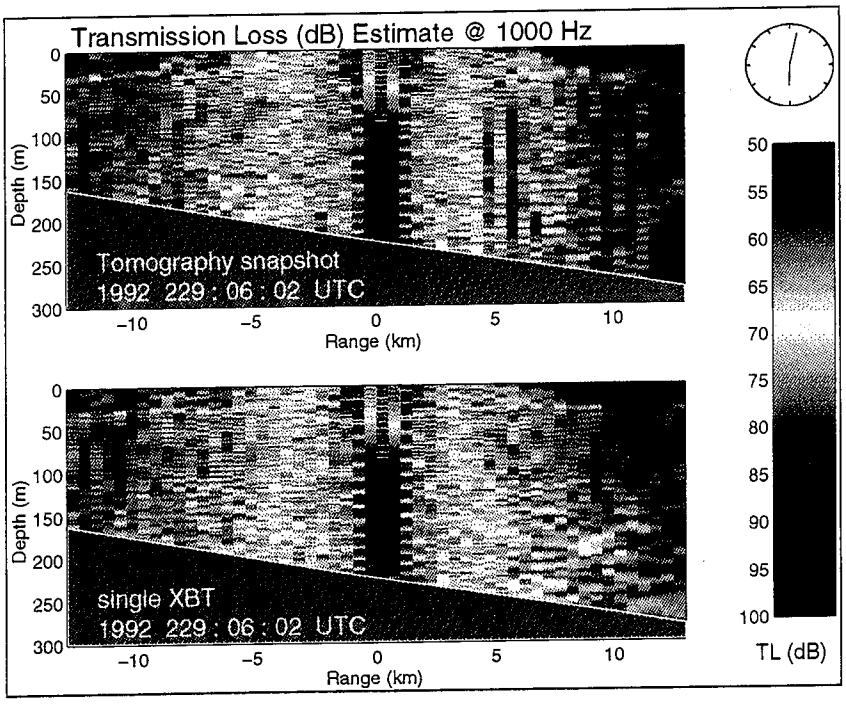
Transmission Loss (dB) Estimate @ 1000 Hz
Depth (m)
Tomography snapshot
1992 229 : 06 : 02 UTC
Range (km)
single XBT
1992 229 : 06 : 02 UTC
TL (dB)

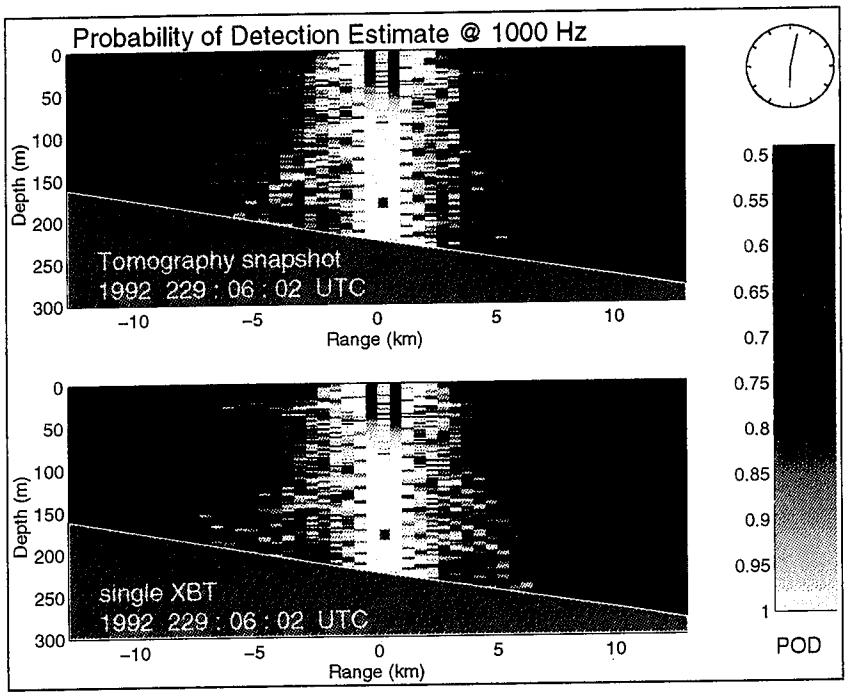
Probability of Detection Estimate @ 1000 Hz
Depth (m)
Tomography snapshot
1992 229 : 06 : 02 UTC
Range (km)
single XBT
1992 229 : 06 : 02 UTC
POD

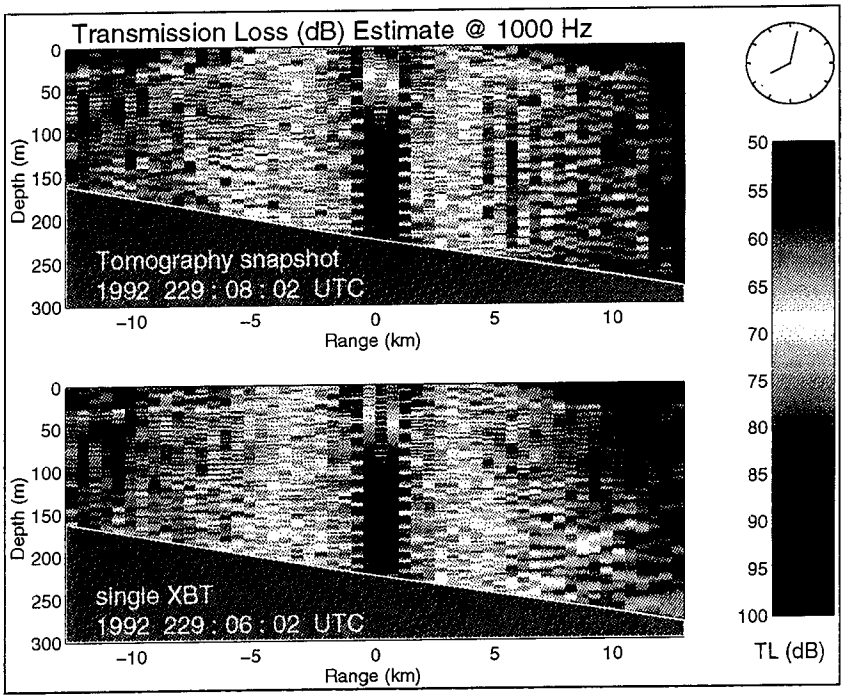
Transmission Loss (dB) Estimate @ 1000 Hz
Depth (m)
Tomography snapshot
1992 229 : 08 : 02 UTC
Range (km)
single XBT
1992 229 : 06 : 02 UTC
TL (dB)

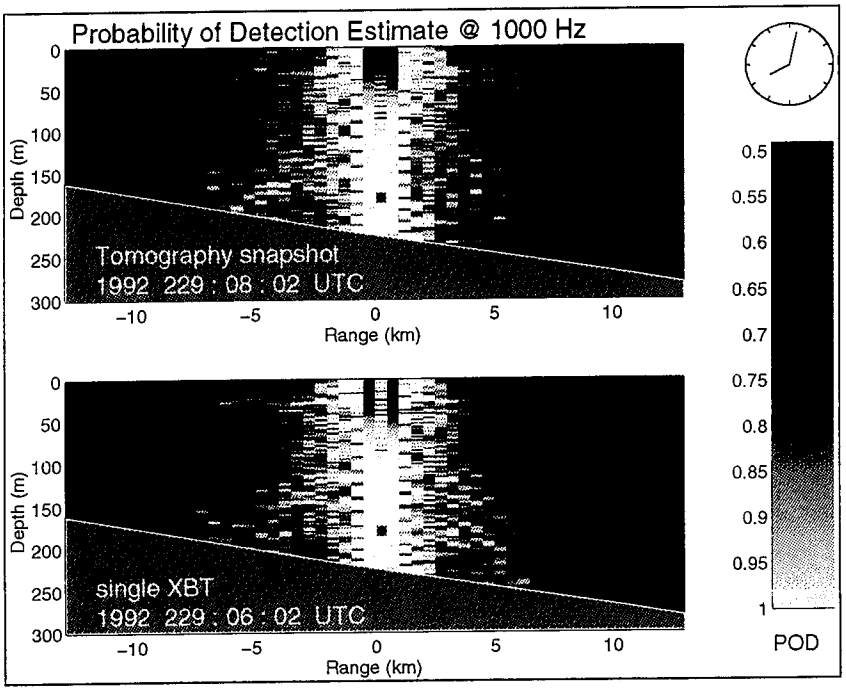
Probability of Detection Estimate @ 1000 Hz
Depth (m)
Tomography snapshot
1992 229 : 08 : 02 UTC
Range (km)
single XBT
1992 229 : 06 : 02 UTC
POD

APPENDIX C. TL AND POD ESTIMATES FOR SOURCE DEPTH 10 METER

This Appendix contains the figures of the transmission loss and probability of detection estimates for the source at a depth of 10 meters. The figures are represented at two-hour intervals. The XBT data is derived from the tomography data at the beginning of the sequence (Figure 3) and at six-hour intervals, starting at midnight.

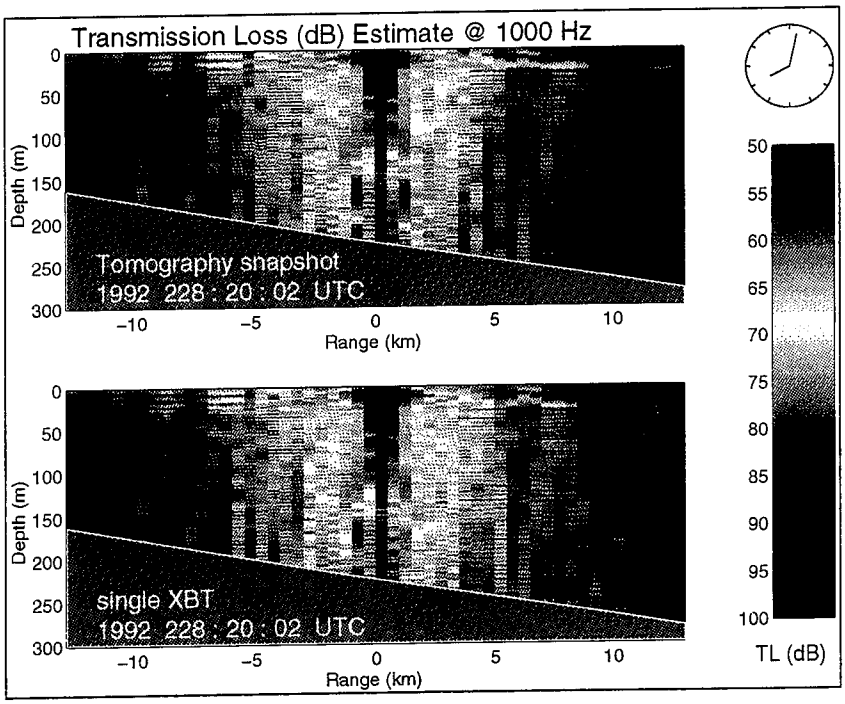
Transmission Loss (dB) Estimate @ 1000 Hz
Depth (m)
0
50
100
150
200
250
300
Tomography snapshot
1992 228 : 20 : 02 UTC
−10
−5
0
5
10
Range (km)
single XBT
1992 228 : 20 : 02 UTC
50
55
60
65
70
75
80
85
90
95
100
TL (dB)

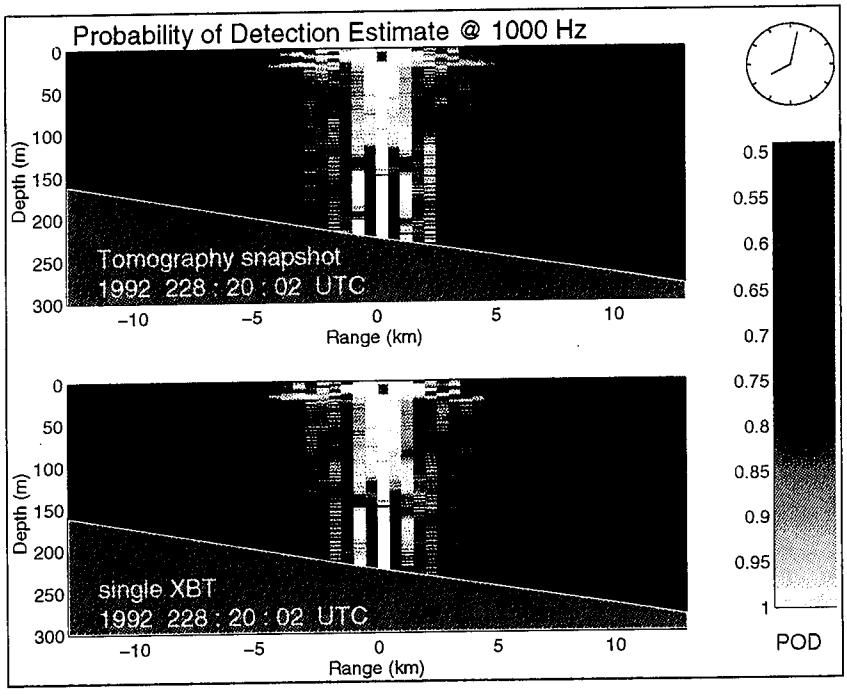
Probability of Detection Estimate @ 1000 Hz
Depth (m)
0
50
100
150
200
250
300
Tomography snapshot
1992 228 : 20 : 02 UTC
−10
−5
0
5
10
Range (km)
single XBT
1992 228 : 20 : 02 UTC
0.5
0.55
0.6
0.65
0.7
0.75
0.8
0.85
0.9
0.95
1
POD

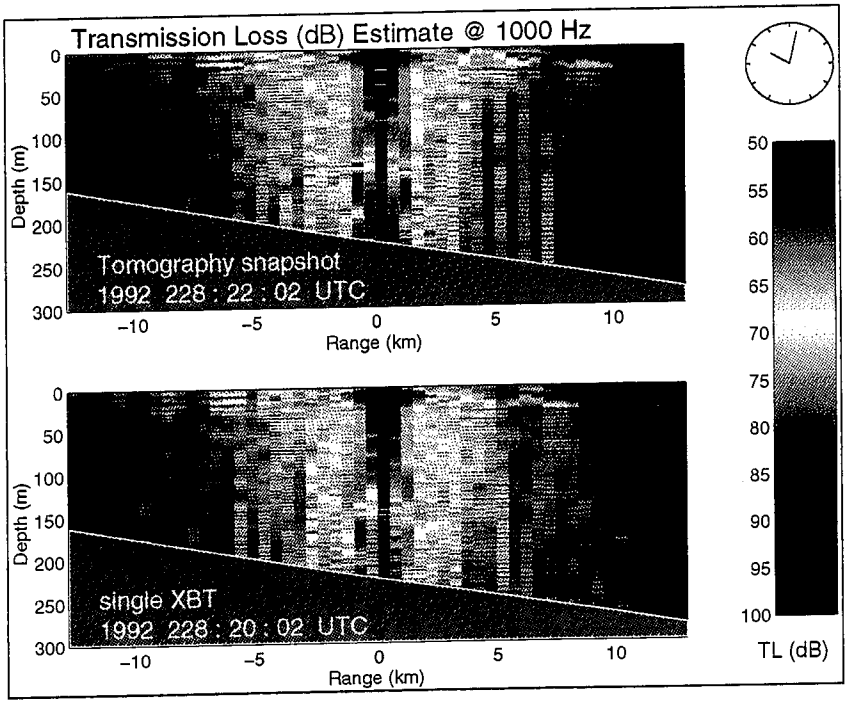
Transmission Loss (dB) Estimate @ 1000 Hz
Depth (m)
0
50
100
150
200
250
300
Tomography snapshot
1992 228 : 22 : 02 UTC
−10
−5
0
5
10
Range (km)
single XBT
1992 228 : 20 : 02 UTC
50
55
60
65
70
75
80
85
90
95
100
TL (dB)

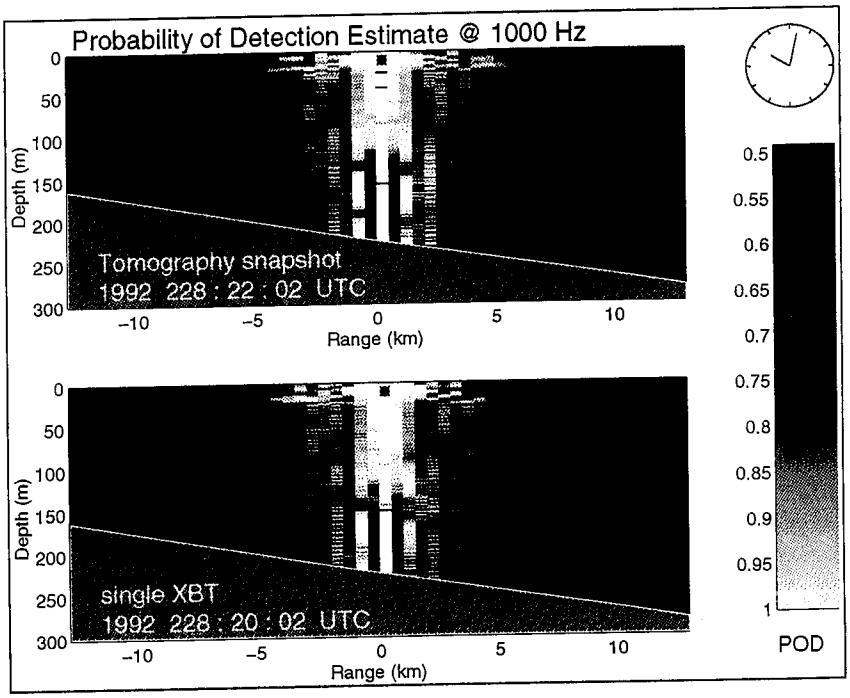
Probability of Detection Estimate @ 1000 Hz
Depth (m)
0
50
100
150
200
250
300
Tomography snapshot
1992 228 : 22 : 02 UTC
−10
−5
0
5
10
Range (km)
single XBT
1992 228 : 20 : 02 UTC
0.5
0.55
0.6
0.65
0.7
0.75
0.8
0.85
0.9
0.95
1
POD

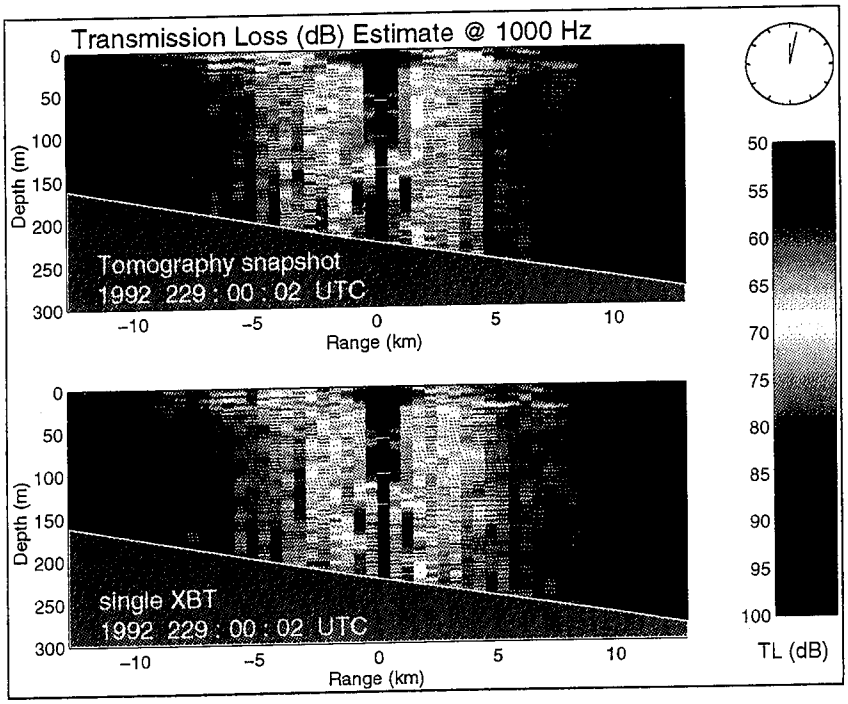
Transmission Loss (dB) Estimate @ 1000 Hz
Depth (m)
0
50
100
150
200
250
300
Tomography snapshot
1992 229 : 00 : 02 UTC
−10
−5
0
5
10
Range (km)
single XBT
1992 229 : 00 : 02 UTC
50
55
60
65
70
75
80
85
90
95
100
TL (dB)

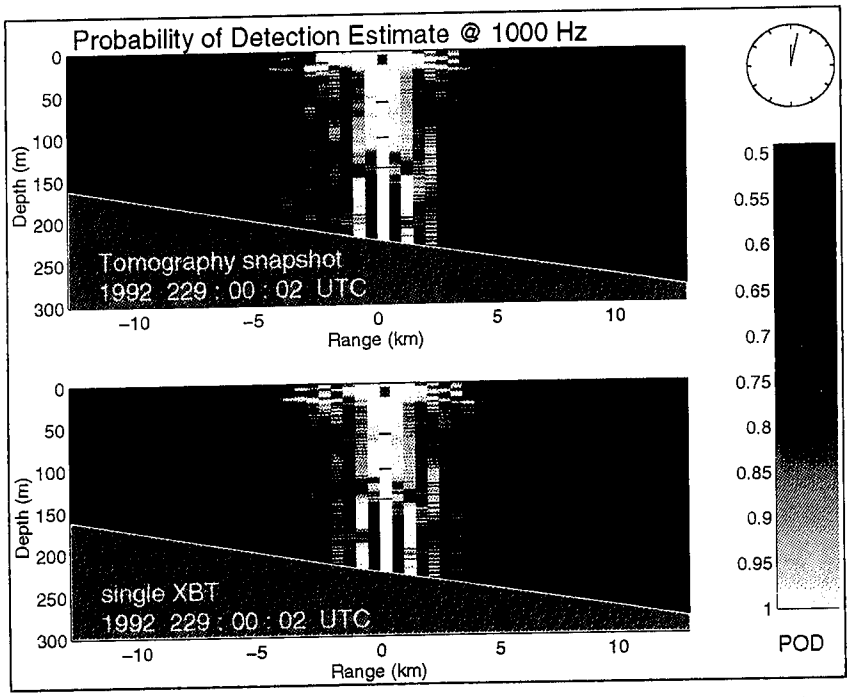
Probability of Detection Estimate @ 1000 Hz
Depth (m)
0
50
100
150
200
250
300
Tomography snapshot
1992 229 : 00 : 02 UTC
−10
−5
0
5
10
Range (km)
single XBT
1992 229 : 00 : 02 UTC
0.5
0.55
0.6
0.65
0.7
0.75
0.8
0.85
0.9
0.95
1
POD

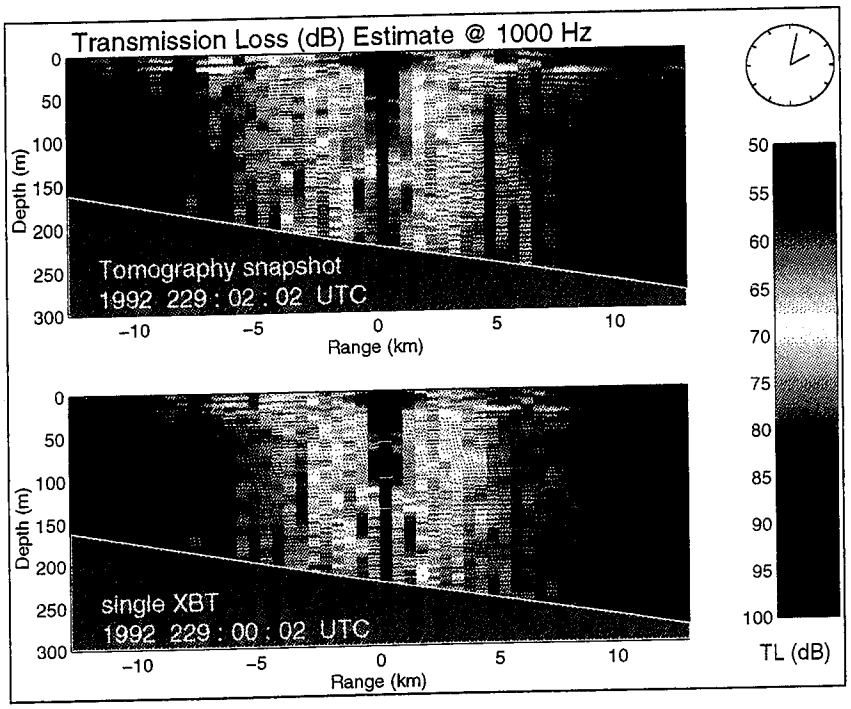
Transmission Loss (dB) Estimate @ 1000 Hz
Depth (m)
0
50
100
150
200
250
300
Tomography snapshot
1992 229 : 02 : 02 UTC
−10
−5
0
5
10
Range (km)
single XBT
1992 229 : 00 : 02 UTC
50
55
60
65
70
75
80
85
90
95
100
TL (dB)

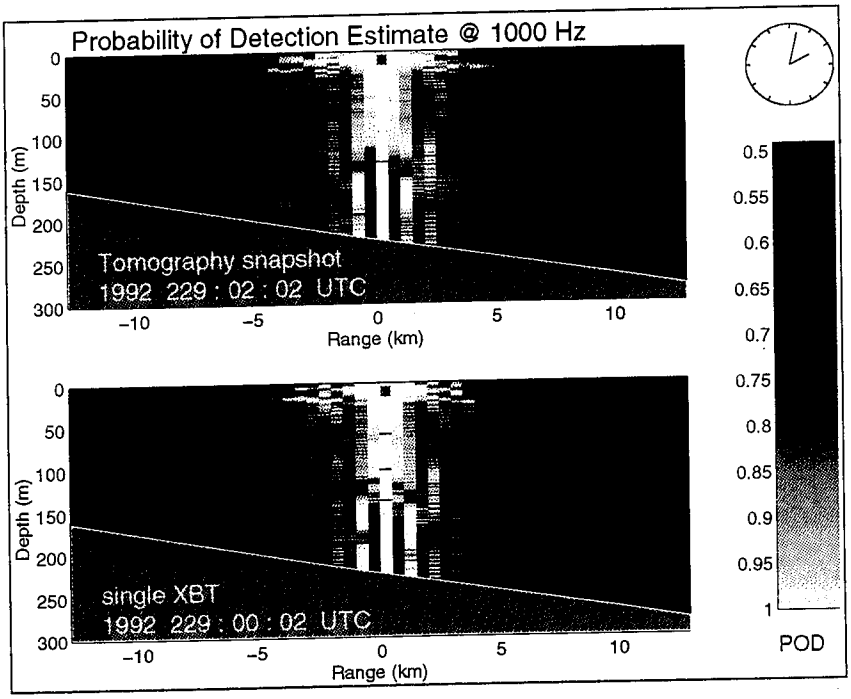
Probability of Detection Estimate @ 1000 Hz
Depth (m)
0
50
100
150
200
250
300
Tomography snapshot
1992 229 : 02 : 02 UTC
−10
−5
0
5
10
Range (km)
single XBT
1992 229 : 00 : 02 UTC
0.5
0.55
0.6
0.65
0.7
0.75
0.8
0.85
0.9
0.95
1
POD

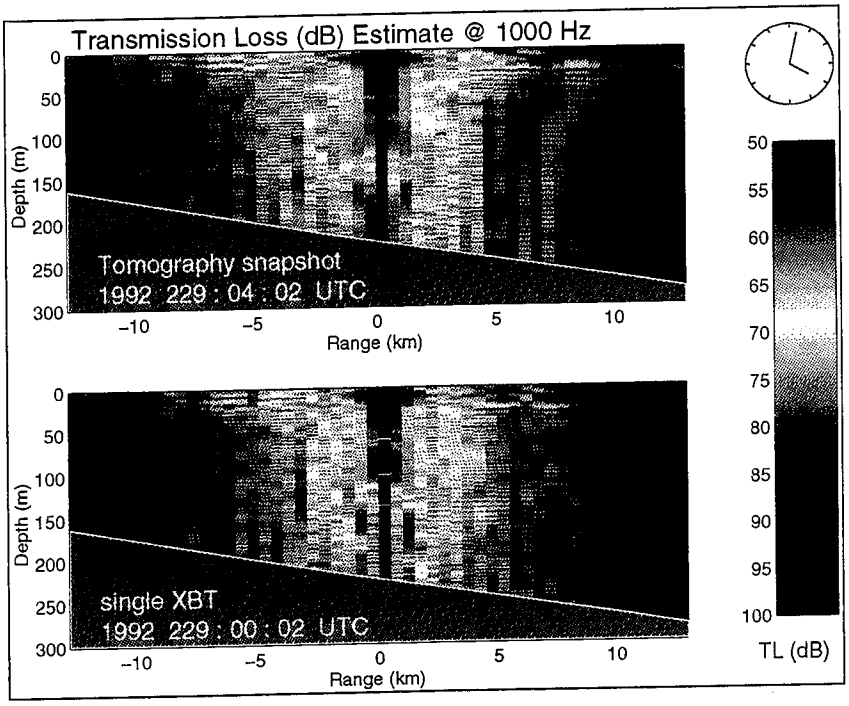
Transmission Loss (dB) Estimate @ 1000 Hz
Depth (m)
0
50
100
150
200
250
300
Tomography snapshot
1992 229 : 04 : 02 UTC
−10
−5
0
5
10
Range (km)
single XBT
1992 229 : 00 : 02 UTC
50
55
60
65
70
75
80
85
90
95
100
TL (dB)

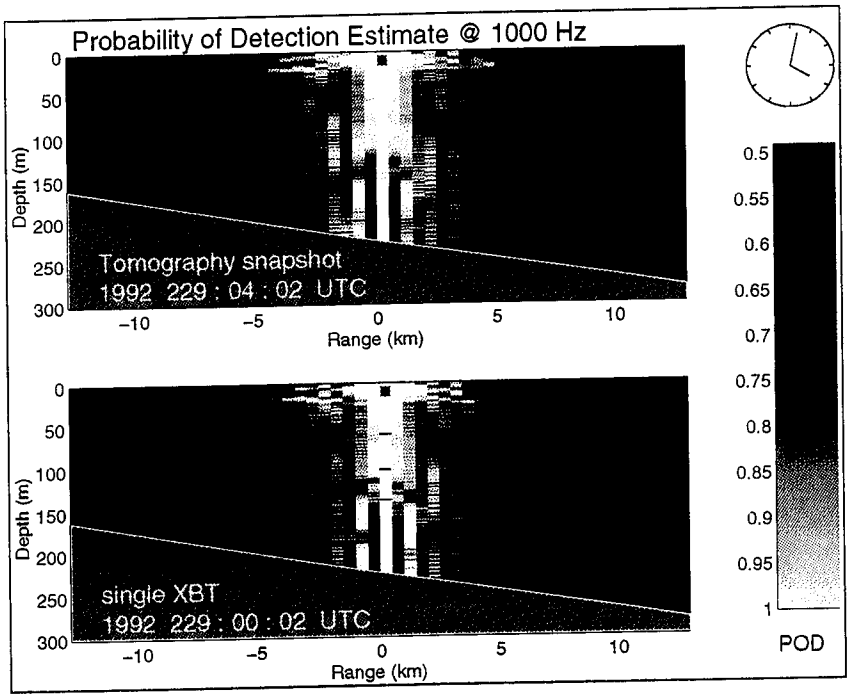
Probability of Detection Estimate @ 1000 Hz
Depth (m)
0
50
100
150
200
250
300
Tomography snapshot
1992 229 : 04 : 02 UTC
−10
−5
0
5
10
Range (km)
single XBT
1992 229 : 00 : 02 UTC
0.5
0.55
0.6
0.65
0.7
0.75
0.8
0.85
0.9
0.95
1
POD

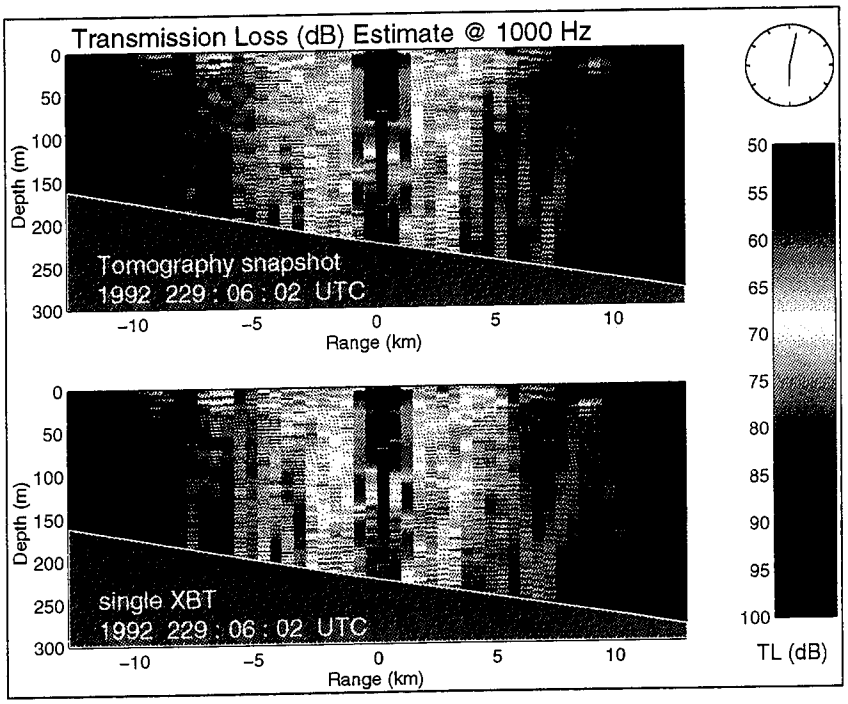
Transmission Loss (dB) Estimate @ 1000 Hz
Depth (m)
0
50
100
150
200
250
300
Tomography snapshot
1992 229 : 06 : 02 UTC
−10
−5
0
5
10
Range (km)
single XBT
1992 229 : 06 : 02 UTC
50
55
60
65
70
75
80
85
90
95
100
TL (dB)

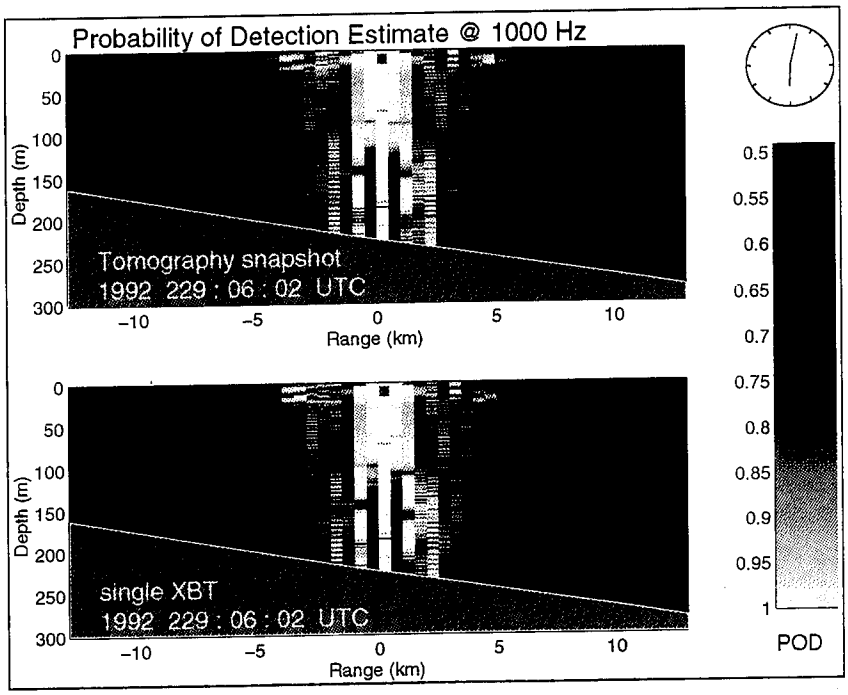
Probability of Detection Estimate @ 1000 Hz
Depth (m)
0
50
100
150
200
250
300
Tomography snapshot
1992 229 : 06 : 02 UTC
−10
−5
0
5
10
Range (km)
single XBT
1992 229 : 06 : 02 UTC
0.5
0.55
0.6
0.65
0.7
0.75
0.8
0.85
0.9
0.95
1
POD

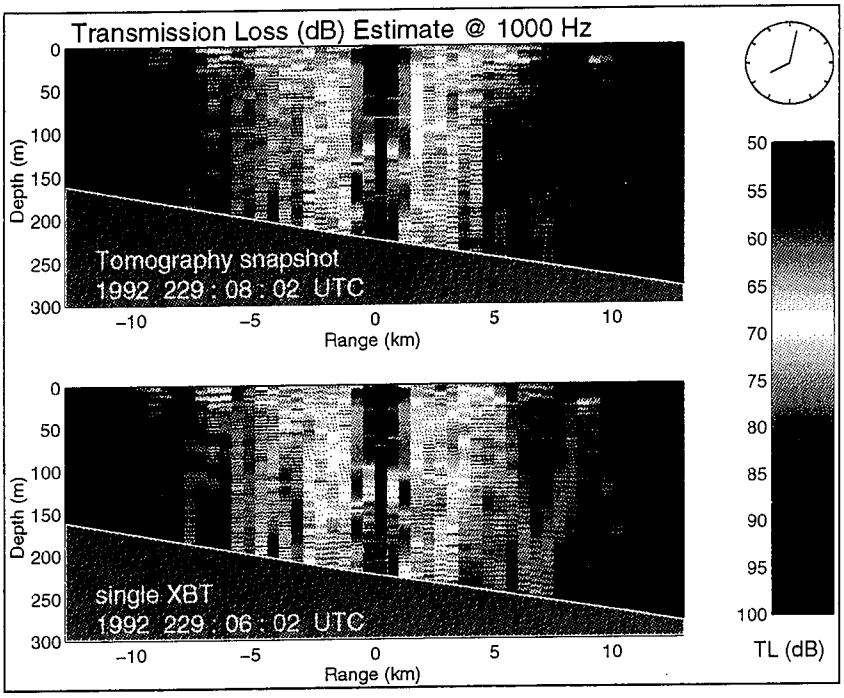
Transmission Loss (dB) Estimate @ 1000 Hz
Depth (m)
0
50
100
150
200
250
300
Tomography snapshot
1992 229 : 08 : 02 UTC
−10
−5
0
5
10
Range (km)
single XBT
1992 229 : 06 : 02 UTC
50
55
60
65
70
75
80
85
90
95
100
TL (dB)

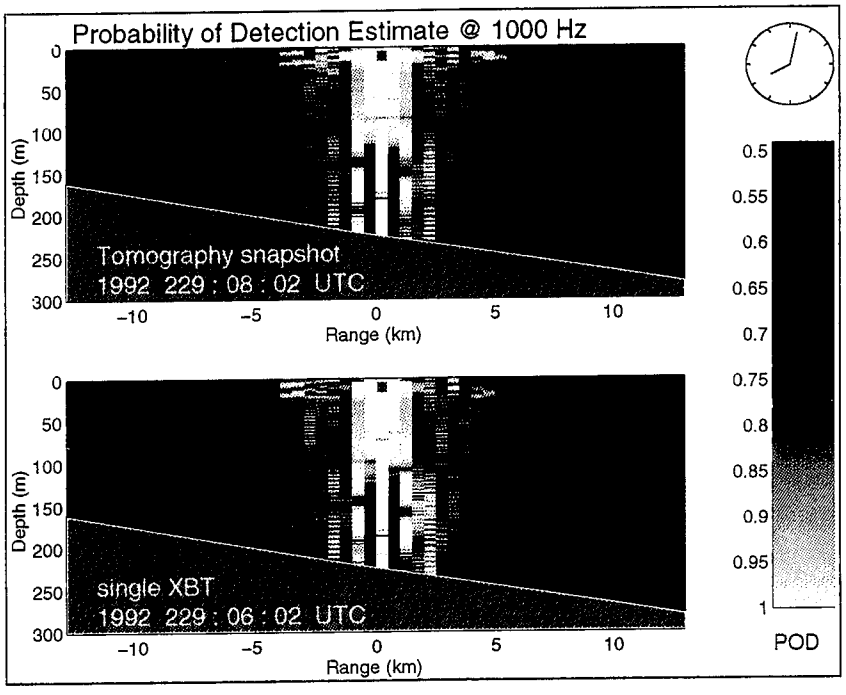
Probability of Detection Estimate @ 1000 Hz
Depth (m)
0
50
100
150
200
250
300
Tomography snapshot
1992 229 : 08 : 02 UTC
−10
−5
0
5
10
Range (km)
single XBT
1992 229 : 06 : 02 UTC
0.5
0.55
0.6
0.65
0.7
0.75
0.8
0.85
0.9
0.95
1
POD

INITIAL DISTRIBUTION LIST

		No. Copies
1.	Defense Technical Information Center Cameron Station Alexandria, Virginia 22304-6145	2
2.	Library, Code 52 Naval Postgraduate School Monterey, California 93943-5101	2
3.	Prof. A.A. Atchley, Code PH/Ay Department of Physics Naval Postgraduate School Monterey, California 93943-5000	1
4.	Prof. J.H. Miller, Code EC/Mr Department of Electrical and Computer Engineering Naval Postgraduate School Monterey, California 93943-5121	5
5.	Prof. C.-S. Chiu, Code OC/Ci Department of Oceanography Naval Postgraduate School Monterey, California 93943-5000	1
6.	Dr. W.W. Denner EOS Research Associates 200 Camino Aguajito, Suite 202 Monterey, California 93940	1
7.	Flagofficer Royal Netherlands Naval College Attn: ir J.A.J. Biemond Postbus 10000 1780 AC Den Helder, the Netherlands	1
8.	Ministry of Defense Directorate Material Royal Netherlands Navy Department of Weapon and Communication Systems OSAO, Wetenschappelijk Medewerker Postbus 20702 2500 ES 's-Gravenhage, the Netherlands	1
9.	Commanding Officer HNLMS Van Galen Attn: LCDR J. Franken Postbus 10000 1780 AC Den Helder, the Netherlands	2

10. TNO Physics and Electonics Laboratory — 1
    Physics and Acoustics Systems Division
    Acoustics Systems Group
    Attn: Dr. G.W.M. van Mierlo
    Postbus 96864
    2509 JG 's-Gravenhage, the Netherlands

11. TNO Physics and Electonics Laboratory — 1
    Operational Research Division
    Maritime Command & Weapon Systems Group
    Attn: Drs. M.H.M. Delmee
    Postbus 96864
    2509 JG 's-Gravenhage, the Netherlands

12. Dr. J.F. Lynch — 1
    Woods Hole Oceanographic Institution
    Woods Hole, Massachusetts 02543

13. Dr. W. Jobst — 1
    NAVOCEANO, Code 0
    Stennis Space Center, Mississippi 39522

14. Dr. T. Curtin — 1
    Office of Naval Research
    800 North Quincy Street
    Arlington, Virginia 22217-5000

15. Dr. M. Badiey — 1
    Office of Naval Research
    800 North Quincy Street
    Arlington, Virginia 22217-5000

16. Mr. J. Schuster — 1
    CNO Code N87T
    Submarine Security and Technology Branch
    Room 4D534
    Pentagon
    Washington, District of Columbia 20350

17. CDR J. Polcari — 1
    PEO (USW) ASTO
    Undersea Warfare
    2531 Jefferson Davis Highway
    Arlington, Virginia 22242-5169